Applied Geochemistry 79 (2017) 36–51

Contents lists available at ScienceDirect

Applied Geochemistry

journal homepage: www.elsevier.com/locate/apgeochem

Hydrochemical effects of saltwater intrusion in a limestone and dolomitic limestone aquifer in Lebanon

Wisam M. Khadra [a, b, *], Pieter J. Stuyfzand [a, c], Boris M. van Breukelen [d]

[a] Delft University of Technology, Dept. of Geoscience and Engineering, Section Geo-environmental Engineering, PO Box 5048, 2600 GA Delft, The Netherlands
[b] American University of Beirut, Dept. of Geology, PO Box 11-0236, 1107 2020 Riad El-Solh Beirut, Lebanon
[c] KWR Watercycle Research Institute, PO Box 1072, 3430 BB Nieuwegein, The Netherlands
[d] Delft University of Technology, Dept. of Water Management, Section Sanitary Engineering, PO Box 5048, 2600 GA Delft, The Netherlands

A R T I C L E I N F O

Article history:
Received 12 October 2016
Received in revised form
4 February 2017
Accepted 6 February 2017
Available online 10 February 2017

Editorial handling by Prof. M. Kersten.

Keywords:
(Dolomitic) limestone aquifer
Hydro(geo)chemistry
Trace elements
Reactive transport model
Lebanon

A B S T R A C T

This study demonstrates groundwater quality differences between a limestone and a dolomitic limestone, (sub)oxic coastal aquifer in the Eastern Mediterranean (Lebanon), with and without ongoing moderate salinization since the last decades. For this purpose, 8 major and 50 trace elements (TEs) were analyzed in 80 water and 65 rock samples, and interpreted with a quad-fold approach utilizing: (1) nonparametric statistical tests, (2) concentration deviations from ideal conservative freshwater–seawater mixing lines, (3) a new parameter called Mixing Enrichment Factor to assess the mobility of chemical constituents under salinizing conditions, and (4) 1-D dual porosity flow path modeling with PHREEQC. Dissolution/precipitation of $Ca_xMg_ySr_zCO_3$ and cation exchange were the main disclosed hydrogeochemical processes besides minor signs of organic matter oxidation. In the dolomitic limestone aquifer, less carbonate dissolved as compared to the limestone aquifer, partly because of lower pCO_2 in addition to seawater inflow triggering Mg-calcite precipitation by cation exchange. Saltwater intrusion led to mobilization of As, Ba, Cu, Ni, Rb, Sr and U in both aquifers, sometimes likely by cation exchange (e.g. Ba and Sr). Some of these TEs (notably Cu and Ni) recorded higher concentrations in the dolomitic limestone regardless of salinization. Other elements like Al, Be, Ce, Cr, Nb, Pb, V, Y and Zr revealed no or a low mobilization tendency. The concentration of all TEs in groundwater remained below drinking water limits notwithstanding moderate salinization. This classifies carbonate rocks as a weak geogenic source of TEs, whereas encroaching seawater appears to be a more important source.

1. Introduction

Coastal aquifers are known for their complex hydrochemical nature due to (1) different inputs from precipitation, infiltrating rivers, intruding seawater, irrigation return flow, and wastewater infiltration (Stuyfzand, 1999; Post, 2002); (2) additional or intensified processes in the saltwater-freshwater mixing zone such as dissolution/precipitation, ion exchange, and oxidation/reduction (Herman et al., 1985; Magaritz and Luzier, 1985; Stuyfzand, 1993a); (3) changes in permeability and porosity due to enhanced karstification or dolomitization of carbonate aquifers (Wicks and Herman, 1995; Emblanch et al., 2005) or clay mobilization in clastic aquifers (Bradford and Kim, 2010); and (4) urbanization of coastal zones (Porter et al., 1996). Approaches to interpret the hydrochemical evolution of groundwater bodies can be subdivided into 3 main groups: (1) mapping (including the use of water typologies and quality indices (e.g. Matthess, 1982; Stuyfzand, 1999), (2) mass balancing (Plummer and Back, 1980; Plummer et al., 1994; Dai et al., 2006; Stuyfzand, 2011; Parkhurst and Appelo, 2013), and (3) 1-D (Appelo, 1994), 3-D (Prommer et al., 2003) reactive transport or variable-density groundwater flow and solute transport modeling (e.g. Sanford and Konikow, 1989; Simmons et al., 2010).

Studying the behavior of trace elements (TEs) in coastal groundwater flow systems is important because they need to be tested against maximum permissible concentrations (MPCs) of drinking (e.g. Mondal et al., 2010; Al Kuisi et al., 2015; Fiket et al., 2015) or irrigation water (e.g. Shi et al., 2013), and some can be utilized as tracers of either infiltration water, pollution or

* Corresponding author. Delft University of Technology, Dept. of Geoscience and Engineering, Section Geo-environmental Engineering, PO Box 5048, 2600 GA Delft, Netherlands.
E-mail address: w.m.khadra@tudelft.nl (W.M. Khadra).

http://dx.doi.org/10.1016/j.apgeochem.2017.02.005
0883-2927/

geochemical processes (e.g. Stuyfzand, 1993b; Gonneea et al., 2014; O'Connor et al., 2015; Stuyfzand, 2015a; Sun et al., 2015). The behavior of TEs is initially affected by the geochemistry of hosting rocks, but saltwater intrusion and mixing with freshwater may trigger further hydrogeochemical processes, notably dissolution/precipitation and adsorption/desorption. For instance, a carbonate-philic element like Sr is significantly mobilized upon limestone dissolution (Shand and Edmunds, 2008; Lin et al., 2013; Gonneea et al., 2014). Other elements such as, U and Zn have less bonding affinity to carbonates (Shand and Edmunds, 2008; Gonneea et al., 2014), but they may be mobilized by increased O_2 concentrations (for instance due to leakage of oxygenated water via multi-aquifer wells) in limestone and clastic (sandstone, shale, and alluvium) aquifers (Ayotte et al., 2011). Several studies in salinizing sandy aquifers confirm the affinity of TEs to become mobilized, e.g. Ba (Stuyfzand, 1993b), Pb and Hg (Sun et al., 2015), or immobilized, e.g. F, Mo, Rb, V and U (Stuyfzand, 1993b). In carbonate coastal aquifers with varying Ca/Mg host rock composition, the behavior of TEs has not yet been thoroughly tackled, except for a study of the Italian Dolomite Mountains (Frondini et al., 2014); however, salinization was not an issue there.

This paper focuses on water quality differences between limestone and dolomitic limestone aquifers with and without salinization. A (sub)oxic coastal system in the Eastern Mediterranean (Lebanon) is chosen for this purpose. The selected system has been subject to excessive pumping since 1991. This has intensified saltwater encroachment. It is yet at a moderate salinizing stage with maximum seawater fraction <20%. Such carbonate aquifers are inherently complex due to their karstic nature. Many authors have addressed the hydrochemistry of Mediterranean coastal aquifers, e.g. Price and Herman (1991); Pulido-Leboeuf (2004); Tulipano et al. (2005); MED-EUWI (2007); de Montety et al. (2008); Sola et al. (2013); Zghibi et al. (2014); Ben Ammar et al. (2016). In Lebanon, however, hydrochemical studies have applied classical approaches only, like (a) Piper, Schoeller, Durov, and Radial plots (Arkadan, 1999; Khadra, 2003; Korfali and Jurdi, 2007, 2009; Saadeh, 2008), or (b) simple water quality indices (Khadra, 2003; Saadeh, 2008; El-Fadel et al., 2014). Recently, Khadra and Stuyfzand (2014) presented a detailed hydrochemical study of the (dolomitic) limestone Damour coastal aquifer system to the south of Beirut. It included a discrimination scheme to define different groundwater bodies (hydrosomes) and their interbedded hydrochemical zones (facies) in addition to the derivation of baseline quality for main constituents, stable isotopes, and many TEs.

The emphasis in this manuscript is given to the hydrochemical effects induced by saltwater intrusion (SWI) on various major constituents and trace elements in conjunction with potential geochemical differences between limestone and dolomitic limestone units. Four lines of research are followed for this purpose, in logical order of increasing complexity: (1) statistics on 4 water groups (limestone vs. Dolomitic limestone with and without salinization); (2) shifts in concentrations of major ions from ideal seawater and freshwater mixing lines; (3) use of Mixing Enrichment Factor (*MEF*), which is introduced here as a new parameter to assess mobility of chemical constituents when mixing (including salinization) occurs; and (4) 1-D flow path PHREEQC modeling with dual porosity formulation. Lines 1 and 3 analyze many species including TEs, whereas lines 2 and 4 are limited to Na, K, Ca, Mg, SO_4, TIC (or alkalinity), and occasionally Sr. 50 TE (including metals, metalloids, lanthanoids, and actinoids) are considered. Their total amount in groundwater is <0.3% of the total dissolved solids for all analyzed samples. 15 elements provide meaningful indications, whereas the others have concentrations constantly below their minimum detection limit (MDL).

2. Setting and methods

2.1. Site description

The study area spans an area of 60 km^2 along the coastal zone of Lebanon in the Eastern Mediterranean (Fig. 1). It has a humid mesothermal Mediterranean climate characterized by dry summers and relatively mild, moist winters with sunshine abundance. The annual precipitation record over the last 25 years showed a range between 352 and 1163 mm, with an average of 770 mm (Meteorological Service, 2010). Orographic precipitation is enhanced on the western side of the Lebanese mountain range due to humid westerly winds from above the Mediterranean Sea. A climatic cycle with extreme conditions of rainfall or partial drought is expected at a return period of ca. 14 years (Arkadan, 2008).

The geology of the area is shown in Figs. 1 and 2, and the hydrostratigraphic units are described in Table 1. The two main hosting units are the C_{4c}-C_5 dolomitic limestone and the coastal C_6-Q limestone. Their exposed parts have few paved surfaces only, and they are considered as major recharge zones for rainfall. Groundwater then flows westward to discharge in low areas at the sea excluding intercepted volumes by pumping wells. Groundwater recharge of local origin was confirmed by the downgradient hydrochemical patterns in oxidants, pollutants, and the strontium maturity index (Khadra and Stuyfzand, 2014). Water budget components are summarized in Table 2.

The baseline groundwater quality of the main (C_{4c}-C_5) aquifer is typical for dolomitic limestone showing oligohaline-fresh, (sub) oxic, calcareous $CaHCO_3$ water. Hydrochemical conditions in 1979–1980 (i.e. 11 years before excessive pumping started) at Naameh-Haret El Naameh villages in the C_{4c}-C_5 aquifer recorded fresh $CaHCO_3$ water type with 115 mg Cl/L at 1200 m from the shoreline (Khadra, 2003). Water quality has been deteriorating westward due to saltwater intrusion. Salinizing NaCl and $CaCl_2$ waters have been recently recorded at about 1000–1500 m inland (Khadra and Stuyfzand, 2014). The C_6 unit (with ca. 1 m/d hydraulic conductivity) plays a partial role in retarding SWI; however, due to fractures saltwater penetrates and reaches the underlying dolomitic limestone aquifer.

The focus in this study is on the groundwater bodies hosted by the dolomitic limestone (C_{4c}-C_5) and the limestone (C_6-Q) units, which are either fresh (without SWI) or salinized (with SWI). Their mean composition is provided in Table S1 (*Supplementary Material*).

2.2. Data collection

Detailed hydrochemical data on groundwater and seawater is available from Khadra and Stuyfzand (2014). A campaign was also launched to collect rock samples from the different geologic units.

2.2.1. Hydrochemical data

During a campaign in April 2011 Khadra and Stuyfzand (2014) collected 102 samples from pumping wells, the Damour River and the Mediterranean Sea. They cover a broad salinity range, from freshwater (TDS = 350 mg/L) in the east, via brackish groundwater close to the coastline (TDS = 2900 mg/L) to hypersaline water of the Mediterranean Sea (TDS = 38,500 mg/L). They were all analyzed on 4 physical, 73 chemical, and 2 isotopic parameters. The hydrochemical data of 80 samples collected from groundwater in the limestone and the dolomitic limestone units, and the Mediterranean Sea are used for the sake of this study. Information on well purging and data quality control are given by Khadra and Stuyfzand (2014).

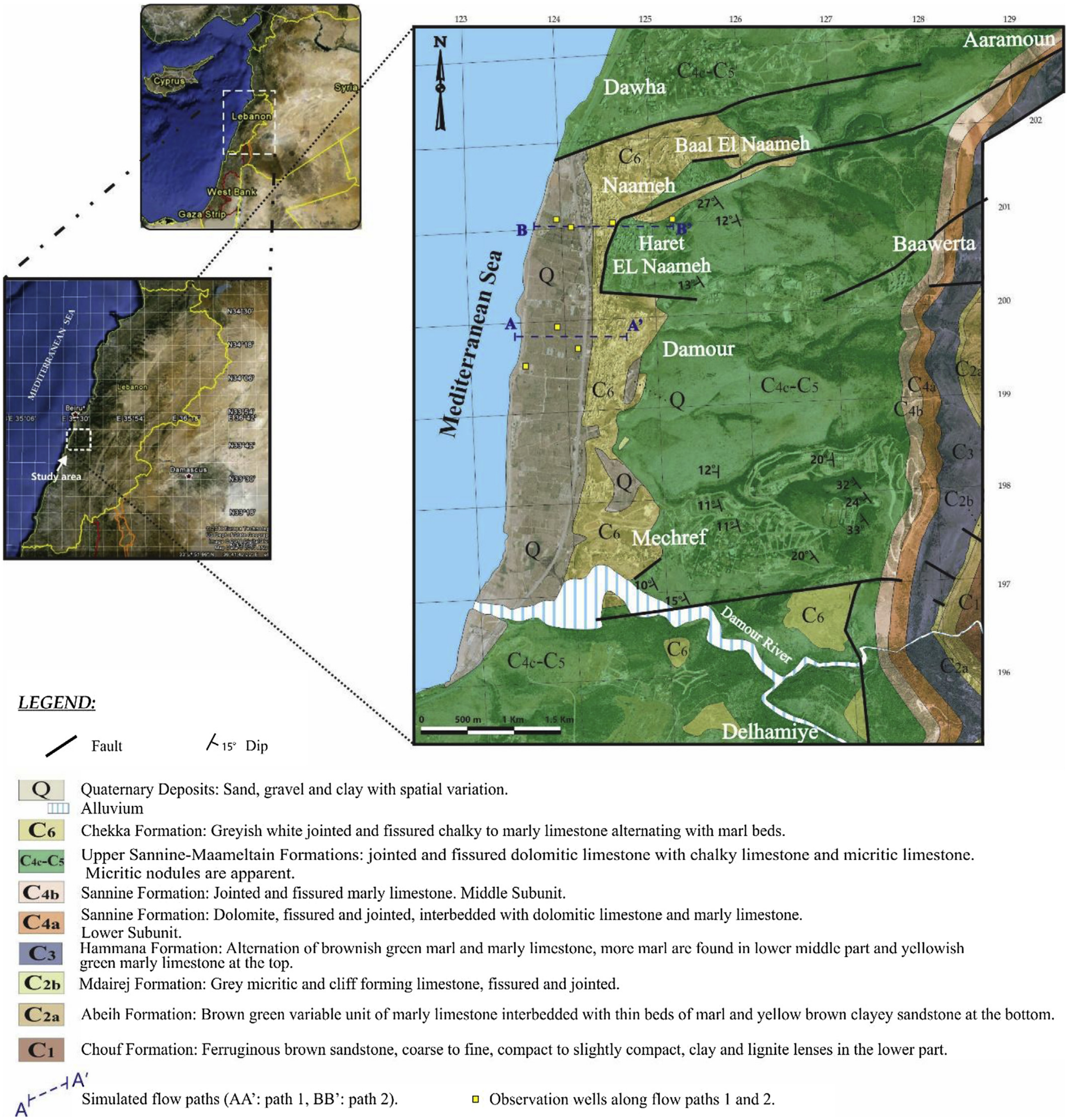

Fig. 1. Geological map of the Damour area (Khadra and Stuyfzand, 2014).

2.2.2. Geochemical analyses

65 samples of fresh rock cuttings were collected from different formations in the study area including aquifers and aquitards at different stratigraphic levels (lower, middle and upper). No preservation was needed because of total elemental analysis. Sampling took into consideration facies variation within the same formation (matrix, fractures and veins). It was not feasible to collect core samples from the current mixing zone because drilling was banned in the area during the study period. The samples were analyzed at AcmeLabs Vancouver on bulk organic matter by LOI, main elemental composition using $LiBO_2$ fusion followed by XRF, 32 rare earth and refractory elements by ICP-MS following a Lithium metaborate/tetraborate fusion and nitric acid digestion, and 14 precious and base metals by ICP-MS after digestion in Aqua Regia. A table including (1) analyzed elements and oxides, (2) relevant methods of analyses, and (3) MDLs, is provided in the *Supplementary Material* (Table S2).

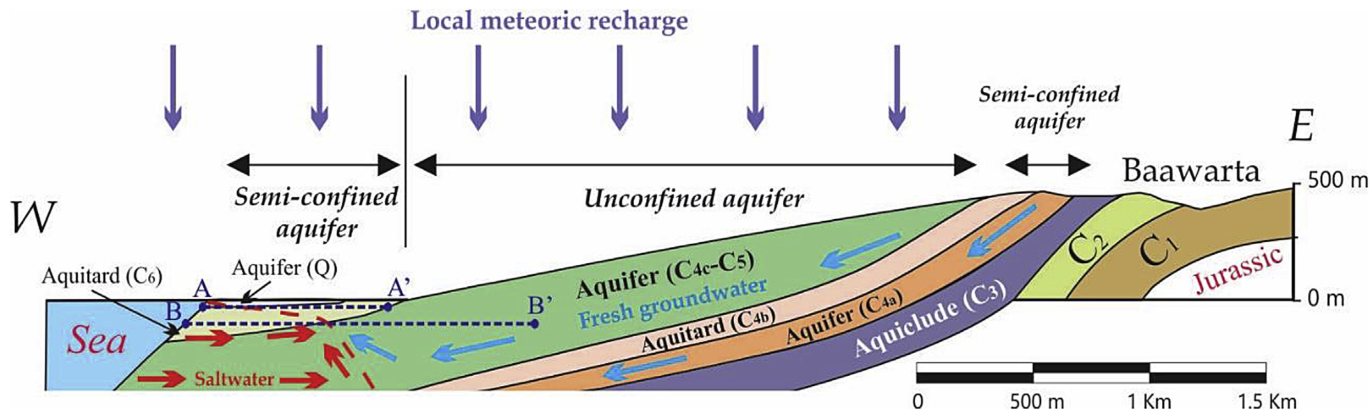

Fig. 2. Hydrogeological cross section of the study area (modified after Khadra and Stuyfzand, 2014). AA′ and BB′ are the simulated unidirectional flow paths from sea to land. Symbols as shown in Fig. 1.

2.3. Statistical methods

Kruskal Wallis H Test and *Mann-Whitney U Test* are two nonparametric tests selected to uncover significance of correlations between independent and dependent variables. The *Kruskal Wallis* is applicable to a group of two and more independent variables, whereas the *Mann-Whitney* tests two population distributions only (Hinkle et al., 2003). They are applied here to check the effect of: (1) saltwater intrusion, and (2) limestone vs. Dolomitic limestone compositional contrast on TEs and major chemical constituents in groundwater. Statistically significant difference is assumed when asymptotic significance is ≤ 0.1, i.e., the null hypothesis is rejected at the 10% significance level. The relatively low stringent level aims at accounting for more possibly affected elements. No concern on mistakenly endorsing a false response because the statistical outcome complements other approaches utilized for the same purpose.

2.4. Sea water input and correction procedure

According to Khadra and Stuyfzand (2014) saltwater intrusion is the main source of salinization in the studied aquifer, and an average Cl/Br ratio of 255 (on mg/L basis) matching the Mediterranean Sea ratio (249) excludes halite dissolution as a potential source of salinization. Hence, the initial step in analyzing the hydrogeochemistry of the mixing zone is to determine the percentage of admixed seawater since geochemical reactivity may vary depending on the extent of salinity and the type of mineral. The solution for 2 end-members, for instance fresh and saltwater, with a single tracer like Cl is:

$$Cl_{MIX} = (1 - f_S)Cl_F + f_S Cl_S \tag{1}$$

$$f_S = (Cl_{MIX} - Cl_F)\,/\,(Cl_S - Cl_F) \tag{2}$$

Where Cl_{MIX} = chloride concentration in mixture [mg/L]; Cl_F = ditto in fresh water [mg/L]; Cl_S = ditto in saline water [mg/L]; f_S = fraction of salt water [−].

The theoretical composition of each salinized groundwater sample as expected for conservative ideal mixing between seawater and freshwater was subsequently quantified and related to the observed composition by using (Fidelibus et al., 1993; Appelo and Postma, 2005):

Table 1
Generalized description of the hydrostratigraphic units in the Damour area from surface to bottom (modified after Khadra and Stuyfzand, 2014).

Hydrogeologic Unit	Geologic Unit	Symbol	Approximate Thickness (m)	Description
Minor aquifer	Quaternary	Q	5	Gravel, sand and clay
Aquitard[a]	Chekka	C_6	160	Chalky to marly limestone
Aquifer	Upper Sannine-Maameltain	C_{4c}-C_5	400	Dolomitic limestone
Aquitard	Middle Sannine	C_{4b}	70	Marly limestone
Aquifer	Lower Sannine	C_{4a}	80	Dolomite and limestone
Aquiclude	Hammana	C_3	200	Marl and marly limestone

[a] It behaves like a minor aquifer due to fractures, fissures and bedding planes.

Table 2
Water balance components estimated for the period April 2001–March 2002 (modified after Khadra and Stuyfzand, 2014).

Component	Value (mm/year)	Value (%)	Area[b] (km^2)	Value (Mm^3/year)
Precipitation	825	100	49	40
Evapotranspiration	327	40	49	16
Run-off	261	32	49	13
Recharge	237	28	49	11
Irrigation return flow[a]	900	Unknown	8	7
Pumped volume	417	25	24	10[c]

[a] Estimate based on land use and average weekly irrigation consumption. The Damour River provides major portion of this water, which is diverted through small canals. % of irrigation return flow out of total precipitation is unknown.
[b] The area excludes residential spots and transportation facilities.
[c] The Q and C_6 units have limited abstraction rates (ca. 0.006 Mm^3/year).

$$C_{TMix} = (1 - f_S) \times C_F + f_S \times C_S \quad (3)$$

$$\Delta C = C_{OBS} - C_{TMix} \quad (4)$$

Where C_{TMix} = concentration of ions in a theoretical mixed sample [mg/L]; C_S = ditto in saline water (presumably seawater) [mg/L]; C_F = ditto in freshwater [mg/L]; C_{OBS} = ditto in observed sample [mg/L].

Ionic delta (denoted by ΔC) reveals whether hydrogeochemical processes other than saltwater mixing contribute to the observed depletion or enrichment (Fidelibus, 2003; Pulido-Leboeuf, 2004; Slama, 2010; Sola et al., 2013; Zghibi et al., 2014; Habtemichael and Fuentes, 2016). This approach is straightforward, provided that end-members can be easily defined. Therefore.

1. It needs to be proven that seawater is the saline end-member. This was accomplished by multi-tracing, e.g., using Eqs. (1) and (2) for more potential tracers like Br and B to confirm seawater origin.
2. The coastal seawater quality needs to be established because it may have changed due to environmental pollution. Knowing the age of seawater intrusion, determined for instance by ^3H-^3He dating or travel times on the basis of a hydrological model, can guide whether the ancient (usually unpolluted) or the recent (possibly polluted) seawater should be used. When historical data is lacking, the ancient seawater quality can be deduced from SMOW corrected by an evapo-concentration factor to the recently measured chloride levels in seawater, and the outcome is then compared for both waters. In this study, the comparison shows only slightly higher Na, As, Ba, Cr, Cu, Ni and V concentrations, having a minor effect on their Mixing Enrichment Factor except for V. Hence, the recent Mediterranean Sea water chemistry is selected.
3. It is not always valid to assume that all freshwaters have the same chemistry (as in previous studies, e.g. Slama, 2010; Habtemichael and Fuentes, 2016; Bouderbala et al., 2016) because different groundwater bodies may exist with large differences in among others Cl, Ca, Mg, and HCO_3. Hence, separate freshwater end-members are assigned throughout this study following the two discriminated groundwater bodies in the limestone and dolomitic limestone units. The 100% mean freshwaters are set to concentrations as derived for the Baseline Groundwater Concentrations (BGCs) of the two aforementioned waters (Khadra and Stuyfzand, 2014).

2.5. Mixing Enrichment Factor

Assuming no other anthropogenic sources to groundwater, Perelman (1972) suggested a migration coefficient "Mig" to assess the mobility of inorganic constituents in groundwater in relation to their concentration in the earth's crust. And recently, Frondini et al. (2014) and Koh et al. (2016) defined and applied an enrichment factor (*EF*; Eq. (5)) to assess the relative mobility of an element based on the ratio to a reference element in the liquid and solid phases; however, EF does not account for groundwater mixing conditions.

$$EF = (C_T/C_R)_L/(C_T/C_R)_A \quad (5)$$

Where C_T = trace element concentration, C_R = reference element concentration (Ca for limestone and Mg for dolomitic limestone), L = liquid phase, and A = hosting aquifer (solid phase).

A new, more versatile coefficient called *MEF* is proposed here to assess the mobility of TEs when mixing with seawater occurs. It is also applicable to main chemical constituents (e.g. Ca, Mg, Na and K), and it can likewise be used to mixing of surface waters (for instance in an estuary) where C_A is applied to suspended material.

$$MEF = 1000\ \Delta C_{MIX}/C_{MAX} \quad (6)$$

With:

$$\Delta C_{MIX} = (1 - f_S)(C_F - BGC_F) + f_S(C_S - BGC_S) \quad (7)$$

$$C_{MAX} = C_A \rho (1 - \varepsilon)/\varepsilon \quad (8)$$

Following Eq. (3),

$$C_F = [(C_{MIX} - (C_S f_S))/(1 - f_S)] \quad (9)$$

We assume $C_S = BGC_S$, so that *MEF* becomes after inserting Eqs. (7)–(9) into Eq. (6):

$$MEF = \frac{C_{MIX} - (C_S \times f_S) - BGC(1 - f_S)}{C_A \times \left(\rho \times \frac{1-\varepsilon}{\varepsilon}\right)} \times 1000 \quad (10)$$

Where *MEF* is the Mixing Enrichment Factor [‰] at a specific salinity fraction $f_S < 1$ (as in Eq. (2)); C_{MIX} = concentration of mixed sample [mg/L]; BGC_F, BGC_S = baseline groundwater concentration of fresh and salt end-member respectively [mg/L]; C_S = concentration of seawater [mg/L]; C_A = content of hosting aquifer [mg/kg]; ρ = specific density of aquifer matrix [kg/L]; and ε = porosity [−].

$[(C_{MIX} - (C_S \times f_S))/(1\text{-}f_S)]$ is the freshwater end-member extracted from the mixed sample based on Eq. (1); $\rho \times (1 - \varepsilon)/\varepsilon$ converts the total content in the aquifer matrix into the maximum theoretical concentration in water when the aquifer matrix would completely dissolve. Therefore, the *MEF* represents the ratio of the mobilized concentration to the maximum theoretical concentration if the aquifer matrix would completely dissolve into the same volume of water. It accounts for the baseline groundwater concentrations, which should be excluded from the impact of (im)mobilization possibly stimulated by SWI because they are entirely natural.

MEF facilitates a quantitative comparison of the behavior of TEs and other constituents in subsurface water. $MEF \geq 0.01$‰ indicates additional mobilization from solid hosting rocks to groundwater solution; *MEF* between −0.01‰ and 0.01‰ indicates that mixing with seawater and natural backgrounds form the exclusive sources of chemical elements in groundwater solution; and a $MEF \leq -0.01$‰ indicates immobilization (loss from solution). The selected ±0.01‰ thresholds are empirical, based on the observed values and their variation. Same thresholds are also applicable to the enrichment factor (*EF*).

The enrichment factors (*EF* and *MEF*) are needed here to complement the statistical methods introduced in section 2.3. They are capable of: (1) defining the behavior of elements (whether mobilized or immobilized), and (2) quantifying the degree of mobilization, unlike the statistical methods that can only discover an interlink between the dependent and the independent variables.

2.6. Forward reactive transport modeling

Forward reactive transport modeling is applied as a predictive approach to simulate the consequences of seawater incursion. PHREEQC-2 (Parkhurst and Appelo, 1999) was used to construct 1-D flow path transport models. The flow is unidirectional from sea to land. One-dimensional simulation was preferred due to limited data and unknown heterogeneities of the aquifer. The major studied aquifer (C_{4c}-C_5) and the overlying C_6 unit are considered dual porous, due to fractures, fissures, bedding planes, and microporous rock matrices. Previous studies on karst aquifers showed that the dispersion model is a good representation of fissured karst systems especially when the mean transit time exceeds 2–3 years (Maloszewski and Zuber, 1985; Maloszewski et al., 2004; Einsiedl et al., 2009). Exchange between the matrix and the semi-stagnant water is assumed to occur via diffusion and reactive transport only (i.e., ignoring advection) unlike for mobile conduits where advection dominates. The simulation then utilizes a first-order exchange approximation with implicit mixing factors $\text{mix}f_m$ and $\text{mix}f_{im}$. They are calculated according to the following equations (Parkhurst and Appelo, 1999, 2013):

$$\text{mix}f_{im} = \frac{\varepsilon_m}{\varepsilon_m + \varepsilon_{im}} \times \left(1 - \exp\left(-\frac{\omega t(\varepsilon_m + \varepsilon_{im})}{\varepsilon_m \times \varepsilon_{im}}\right)\right) \tag{11}$$

$$\text{mix}f_m = \text{mix}f_{im}\frac{\varepsilon_{im}}{\varepsilon_m} \tag{12}$$

Where ε_m is the porosity of mobile zone [−], ε_{im} is the porosity of immobile zone [−], ω is the exchange factor accounting for the exchange between immobile and mobile cells [s^{-1}], and t is the time step [s].

Half of the cells along a flow path (e.g. 300 cells out of 600) are used for mobile groundwater with uniform distribution of stagnant porosity and mixing conditions. An equivalent number +1 cell (i.e. 301) is introduced as an associate in the immobile zone. Each mobile cell (x) exchanges with the immobile cell numbered 300 + 1 + x since cells 302 to 601 are the immobile ones (Parkhurst and Appelo, 2013). The exchange factor is estimated in this study at 1.4e-8 s^{-1} assuming spherical stagnant zone with diffusion coefficient = 6.4e-13 m^2s^{-1}, ε_{im} = 0.08 to 0.12, and a shape factor = 0.21 (Van Genuchten, 1985). Sensitivity of the exchange factor checked for one order magnitude showed minor impact.

Dispersivity estimate relied on the following empirical power law (Schulze-Makuch, 2005):

$$\alpha_L = c(L)^k \tag{13}$$

Where α_L = longitudinal dispersivity [m]; k is a scaling exponent; c is a parameter based on type of geological media [m^{1-k}]; L = flow tube length [m]; k is 0.4 and c is 0.8 for consolidated rocks based on extensive data sets compiled by Schulze-Makuch (2005).

Constraints on time steps and grid size are considered in order to minimize numerical dispersion in fractured bedrock. An advective diffusive flux ratio (ψ) is introduced as a guide in choosing grid spacing and model time steps according to the following equation (Lipson et al., 2007):

$$\psi = \frac{v \times b \times \Delta z}{D_f \times \varepsilon_{\text{im}} \times \Delta x} \tag{14}$$

Where ψ in a fracture is supposed to be > 10; v = average linear groundwater velocity [m^2s^{-1}]; D_f = diffusion coefficient across fracture wall [m^2s^{-1}]; b = fracture aperture [m]; ε_{im} = porosity of immobile zone, i.e. bedrock matrix [−]; Δx = the mobile cell length [m]; Δz = the immobile cell (or macro-pore) length [m], assumed here as 0.001 m (Yan et al., 2015).

The model setup including initial conditions (water chemistry and geochemistry), inflow solution chemistry, and geochemical reactions utilized are explained in the *Results* section.

3. Results

3.1. Geochemistry of hosting rocks

Results of the geochemical analyses of the discerned geological formations are summarized in Table 3, and a graphical output from a Pearson linear correlation matrix is provided in Fig. S1 (see *Supplementary Material*) where main clusters are recognized based on their so-called correlation score plot (Stuyfzand, 2015b). The Lower Sannine Formation (C_{4a}) is enriched in magnesium approaching a dolomite like composition ($Ca_{0.58}Mg_{0.42}Sr_{0.0002}CO_3$) as deduced from major elements; strontium is assumed here as a solid solution impurity. The Middle Sannine Formation is conversely Ca-enriched with $Ca_{0.96}Mg_{0.04}Sr_{0.0002}CO_3$ principal mineralogical composition. It has higher Al, Fe and K content indicating more clay deposition. Lower Al correlation score (Fig. S1) points to its marine origin as also confirmed by clustering of Ca, Mg and Sr; the latter indicates an environment supposedly rich in aragonite and low Mg-calcite.

The C_{4c}-C_5 carbonate rock aquifer, most dominant in the study area, shows high Mg content with $Ca_{0.70}Mg_{0.30}Sr_{0.0003}CO_3$ composition (Table 3). Few samples, however, at mid-levels have Ca-rich micritic limestone, with lowest Si, Al, K and trace elements such as Nb, Rb, Ga, La and Y, which is attributed to lack of non-carbonate impurities (Nader et al., 2006). More traces of silicon appeared at the bottom, upper levels and closer to the sea. Visual inspection of rocks reveals minor coatings and veins of quartz in addition to secondary deposition of chert nodules in addition to some intercalations of clay. The quite low Fe content (0.1 wt. %) could be carbonate-bound or present as ferric hydrous oxide. The two dolomitic units (C_{4a} and C_{4c}-C_5) have the highest Mg content and lowest Ca, Fe, Al, As, Ba and many other TEs (Ce, Co, Cr, Cu, La, Nd, Ni, Sr, V, Y, Yb, Zn, and Zr).

The Chekka Formation (C_6) (overlying the C_{4c}-C_5 unit) has calcite predominance (90%) with ca. 8% clayey composition. The higher level and correlation score of its Ba content (Table 3; Fig. S1) is probably attributed to more illite and/or K-feldspar, and clustering of some TEs like Co, Cu, V and Zn indicates more adsorption on clay minerals like kaolinite or on fine-grained heavy minerals. It also has highest Sr content. The topmost Q unit is characterized by a sequence of uncemented clastic deposits, 69% calcareous fragments ($Ca_{0.94}Mg_{0.06}Sr_{0.0007}CO_3$ composition), in addition to ca. 18% quartz and 10% kaolinite. Presence of some clay or heavy minerals with higher Al-Fe content is inferred from strong correlation between Al_2O_3 and Fe_2O_3 (r = 0.79).

The bulk of the As, Ce, Co, Cu, Ga, La, Nb, Nd, Ni, Rb, V, Y, Yb and Zr contents in the C_6-Q and C_{4c}-C_5 units is probably bound to clay minerals (e.g. kaolinite or illite) or fine-grained heavy minerals (e.g. ilmenite or biotite) as confirmed by the positive correlations these TEs have to Al, K, Fe and Ti (r > 0.6). Some small dark mineral inclusions are clearly visible in the admixtures of clay. These impurities could be remnants of direct weathering of volcanic rocks that occurred in the early Cretaceous (Dubertret, 1955). In addition, volcanism during that episode could have enriched the level of some TEs in seawater (e.g. Ni, Y, and Zr), from which the clays deposited later (Nader, 2000).

Organic matter (OM) is also a well-known host for a range of trace elements (Tribovillard et al., 2004; Pichler and Mozaffari, 2015); however, bivariate correlations of geochemical data show no relation between OM and TEs unlike a clear positive correlation with iron (r > 0.6 between Fe and Al, Be, Ce, Cr, Cu, Ga, Mo, Nd, Ni, U, V, Y, Yb, Zn and Zr). This excludes OM as an apparent source of TEs, and nominates hydrous ferric oxides to be the main traps in clays, since pyrite role is ignored under oxic conditions.

Table 3
Minimum, maximum and median composition of hosting rocks, and the main mineral phases as deduced from XRF and ICP-MS/ES results. The whole data set is provided in Table S3 (see *Supplementary Material*).

Unit		# of samples	BOM	wt %								PPM								
				Ca	Mg	Na	K	Si	Fe	Al	Mn	As	Ba	Be	Ce	Co	Cr	Cu	Ga	La
Q	min	5	0.6	24.0	0.3	0.01	0.05	8.3	1.3	0.8	0.02	2.7	35	1.0	9.7	3.9	34	4.4	1.3	5.7
	max		2.7	29.2	4.3	0.04	0.08	10.3	2.7	1.7	0.03	5.2	163	5.0	17.5	7.8	130	25.2	3.5	14.5
	median		2.1	28.2	0.4	0.02	0.05	9.6	1.7	1.1	0.02	3.6	39	5.0	11.6	4.4	34	6.7	2.4	7.8
C_6	min	8	0.6	33.7	0.2	0.01	0.00	1.1	0.3	0.4	<0.01	0.6	33	1.0	4.9	0.8	34	11.2	0.6	7.4
	max		1.9	38.3	0.3	0.05	0.02	4.1	0.8	1.3	<0.01	5.7	411	3.0	12.1	2.3	185	41.4	2.2	13.3
	median		1.2	36.3	0.2	0.02	0.00	2.2	0.5	0.9	<0.01	3.5	41	2.0	8.4	2.0	85	30.1	1.8	10.4
C_{4c}-C_5	min	28	0.0	2.1	0.3	0.01	0.00	0.1	0.0	0.0	0.01	0.5	2	1.0	0.3	0.2	7	0.3	0.6	0.2
	max		3.4	39.7	12.6	0.04	0.07	41.9	0.4	0.7	0.04	4.0	23	3.0	8.4	2.4	68	7.1	0.9	5.0
	median		0.1	24.5	10.4	0.02	0.02	0.5	0.1	0.1	0.01	1.0	7	3.0	1.7	0.6	21	1.6	0.8	1.3
C_{4b}	min	3	0.7	26.4	0.5	0.02	0.03	1.1	0.2	0.4	0.01	0.9	12	1.0	2.5	1.3	27	2.3	1.8	2.1
	max		6.6	38.2	1.4	0.02	0.59	7.7	1.7	2.8	0.01	8.6	46	3.0	11.2	3.9	198	10.2	5.2	7.7
	median		2.7	34.8	1.1	0.02	0.06	2.5	1.0	0.9	0.01	6.1	19	2.0	3.8	2.8	82	10.2	3.5	2.3
C_{4a}	min	21	0.1	15.2	5.2	0.01	0.00	0.1	0.0	0.0	0.01	0.5	2	1.0	0.5	0.3	7	0.5	0.5	0.3
	max		1.1	31.7	13.1	0.06	1.13	7.8	2.0	3.3	0.01	5.9	45	5.0	22.9	4.8	123	11.3	7.7	12.8
	median		0.1	21.9	12.3	0.02	0.02	1.0	0.3	0.3	0.01	2.4	7	2.5	3.0	1.4	21	1.6	1.1	1.6

Unit		PPM													Deduced major mineral phases (wt %)		
		Mo	Nb	Nd	Ni	Pb	Rb	Sr	U	V	Y	Yb	Zn	Zr	**$Ca_xMg_ySr_zCO_3$**	Quartz	Kaolinite[a]
Q	min	0.2	2.9	4.2	8.4	1.4	4.5	174	1.2	22	6.6	0.6	13.0	38.5			
	max	0.6	6.4	10.7	28.4	4.4	9.4	761	4.9	52	23.2	1.6	64.0	58.6			
	median	0.4	4.5	7.6	11.0	1.9	6.5	218	1.5	47	8.2	0.6	21.0	49.2	$Ca_{0.94}Mg_{0.06}Sr_{0.0007}CO_3$	17.7	9.5
C_6	min	0.1	0.7	4.8	5.4	0.9	2.0	824	1.2	20	10.9	0.5	13.0	11.6			
	max	1.4	2.2	8.8	40.3	2.3	4.5	1133	7.9	67	23.7	1.5	81.0	22.7			
	median	0.3	1.6	6.9	16.2	1.9	3.8	975	2.5	45	16.8	1.1	35.0	17.7	$Ca_{0.99}Mg_{0.01}Sr_{0.0018}CO_3$	2.7	8.9
C_{4c}-C_5	min	0.1	0.1	0.4	0.5	0.2	0.5	28	0.3	9	0.3	0.1	1.0	0.6			
	max	3.5	2.2	3.2	8.4	29.7	9.8	241	3.1	27	4.6	0.3	26.0	23.6			
	median	0.2	0.6	1.1	1.2	0.6	1.9	160	1.2	16	1.3	0.1	5.0	4.5	$Ca_{0.70}Mg_{0.30}Sr_{0.0003}CO_3$	0.6	1.4
C_{4b}	min	0.2	0.9	1.5	11.0	0.3	4.0	75	1.1	12	1.1	0.1	6.0	6.8			
	max	0.5	5.4	3.6	18.8	1.6	32.8	227	2.1	128	3.9	0.4	19.0	41.0			
	median	0.4	3.7	1.6	14.9	1.0	16.4	76	1.3	62	1.8	0.1	12.0	30.4	$Ca_{0.96}Mg_{0.04}Sr_{0.0002}CO_3$	3.4	8.1
C_{4a}	min	0.1	0.1	0.3	0.5	0.2	0.4	73	0.7	10	0.2	0.1	1.0	1.1			
	max	5.0	13.4	11.2	39.2	1.5	38.8	168	3.9	117	7.7	0.8	19.0	119.1			
	median	0.3	1.2	1.4	4.5	0.6	3.8	97	1.6	20	1.3	0.2	3.5	9.8	$Ca_{0.58}Mg_{0.42}Sr_{0.0002}CO_3$	1.6	2.5

[a] Al was assumed to derive from kaolinite, justified by low K content in Q, C_6 and C_{4c}-C_5 formations although small amounts could be attributed to other sources (like feldspars) probably existing in the C_{4b} and the C_{4a} units. Kaolinite took part of Si, and the remaining was attributed to quartz.

3.2. Statistical results

Using the statistical software package *SPSS*, the *Kruskal Wallis H Test* was utilized to determine whether 23 dependent variables (Na, K, Ca, Mg, SO_4, TIC, Fe, Si, Al, As, Ba, Be, Co, Cr, Cu, Mo, Ni, Pb, Rb, Sr, U, V and Zn) have statistically significant differences among 4 water groups hosted by: (1) limestone, (2) limestone with SWI, (3) dolomitic limestone, and (4) dolomitic limestone with SWI. Results reveal statistical differences for the 6 main constituents (Na, K, Ca, Mg, SO_4 and Fe) and 10 TE (As, Ba, Be, Co, Cu, Ni, Rb, Sr, U and V) indicating that salinization and/or geochemical contrast (between limestone and dolomitic limestone) do have an effect on their variance with different effect size (Table S4, *Supplementary Material*). In contrast, Al, Cr, Mo, Pb, Zn, and TIC are not affected. The *Mann-Whitney U Test* then determines specifically which variable is responsible for the recorded difference (Is it SWI or compositional contrast?). In fact, Na, K, Si, SO_4 and some TEs (As, Ba, Cu, Rb, Sr and U) show variance between limestone and dolomitic limestone even under freshwater conditions whereas salinization poses an effect on Na, Ca, SO_4, U and V concentrations for both geochemistries. K, Mg, As, Ba, Cu, Ni, Rb and Sr are affected by SWI in the dolomitic limestone only (Table S5, *Supplementary Material*). Be, Co and Fe are influenced by the dual impact of geochemistry and SWI; otherwise they are not affected separately.

3.3. Chemical equilibria

Most samples show undersaturation with respect to aragonite, dolomite, siderite, witherite, strontianite and barite; supersaturation of silicate minerals (e.g. kaolinite); and near equilibrium with calcite and Mg-calcite. Few samples on the western rim of Dawha village have (Mg)calcite, aragonite, and dolomite oversaturation. Halite and gypsum were not observed in the rock samples, while the water is strongly undersaturated. Average pCO_2 of fresh groundwater in the dolomitic limestone and limestone units record $10^{-1.7}$, and $10^{-1.4}$ atm, respectively. They show higher than average values mentioned for carbonate aquifers by Drever (1997) and Langmuir (1997) ($10^{-2.5}$ - 10^{-2} atm), but a similar range was observed elsewhere, e.g. East Anglia, U.K (Heathcote, 1985), and Drahany Highlands, Czech Republic (Faimon et al., 2012). Worldwide patterns of pCO_2 depend on climatic conditions (temperature and rainfall), and according to Brook et al. (1983) the Eastern Mediterranean area has pCO_2 range on land from $10^{-2.6}$ to $10^{-2.2}$. Nevertheless, the discrepancy in pCO_2 observed in the studied groundwater points toward more uptake of CO_2 from root respiration and oxidation of organic matter probably buried with limestone weathering products (Faimon et al., 2012).

Ionic deltas (ΔC) were calculated for major ions (Na, Ca, Mg and SO_4), TIC and Sr (due to its incorporation into $CaCO_3$). Subsequently, the samples were discerned based on formations from which they derive, the limestone C_6-Q and the dolomitic limestone C_{4c}-C_5 units. Excellent correspondence of saltwater fraction calculated for chloride and with multi-tracing using Eqs. (1) and (2) for Br, B, Na and SO_4 confirm that the seawater is the saline end-member. On the other hand, two freshwater end-members were assigned separately for the second end-member as derived for the baseline groundwater concentrations in the limestone and the dolomitic limestone (the BGCs are provided in Table 4). Noteworthy that salt sources like halite dissolution, connate old sea water with altered composition, and recent irrigation return flows or sewage effluent are nearly absent as confirmed from bivariate plots and correlation matrices of NO_3 against EC, Cl, Ca and Mg (Khadra and Stuyfzand, 2014).

Plots of ΔNa, ΔCa, ΔMg, ΔTIC and ΔSr (calculated using Eq. (4)) versus seawater fraction (Fig. 3) show different processes revealing departure from ideal seawater-freshwater mixing. ΔTIC exhibits a dominant enrichment in both aquifers pertaining to carbonate dissolution predominance. Simultaneously all samples are Na depleted with respect to the theoretical mixing line, and the depletion increases with salinity. Ca is conversely enriched for most samples with reasonable correlation to seawater fraction. This is a typical behavior in salinized groundwater and common for both formations (limestone and dolomitic limestone) conforming to Na/Ca cation exchange. However, the steeper slope of Na and Ca in the limestone samples testifies of more exchange with salinity owing to higher exchange capacity (see Table 6). In addition, part of Ca stronger increase pertains to more calcite dissolution in the limestone rocks, partly due to higher pCO_2, and subsequently lower pH and $SI_{calcite}$, in the coastal plain region compared to the mountains. pCO_2 relative rise is probably attributed to higher vegetation density and higher temperature. Mg records a different trend; it is mostly enriched in the dolomitic limestone aquifer, but depleted in most limestone samples (Fig. 3). This is due to more Mg release by dissolution from Mg-rich hosting rocks, and occasional exchange of Na (and K) for Mg.

Sr shows a steeper slope in the limestone unit, which reflects the better Sr fit into pure $CaCO_3$ than in dolomitic limestone. This is also confirmed from the observed ascending trends of Ca, Sr and TIC in the limestone unit. SO_4 ionic deltas show dominance of near conservative mixing conditions for the C_{4c}-C_5 units, whilst enrichment prevails for the limestone samples. This latter anomaly is probably related to atmospheric inputs and/or some agrochemicals applied in the overlying quaternary sand unit, which is a main cultivation strip.

3.4. Seawater mixing effect

The mixing between intruding seawater and ambient freshwater probably induced a new hydrochemical equilibrium affecting the behavior of major constituents and some trace elements. Few groundwater samples with Al > 10 μg/L in near pH neutral water were eliminated a priori due to probable filtration bias (Stuyfzand,

Table 4
Sources and behavior of TEs and major constituents in the 2 discerned geochemistries, limestone (C_6-Q) and dolomitic limestone (C_{4c}-C_5) for fresh and salinized groundwater.

TE	Predominant ionic form	Main aquifer source	Aquifer geochemistry		Seawater	Hydrochemistry of salinized groundwater		BGC[a]		*EF*, fresh groundwater (BGC)		*MEF*, salinized groundwater	
			mg/kg		μg/L					0% f_S	0% f_S	1% f_S	7.5% f_S
	(sub)oxic conditions		*C_6+Q (L.S)*	*C_{4c}-C_5 (Dol. L.S)*	*S*	*L.S*	*Dol. L.S*	*L.S*	*Dol. L.S*	*L.S*	*Dol. L.S*	*L.S*	*Dol. L.S*
Na	Na+	$NaAlSi_3O_8$	300	200	11569000	67,450	183,600	37,700	11,200	278.67	95.95	−13.55	−54.06
K	K+	$KAlSi_3O_8$	400	200	467,000	4000	7600	2400	1300	13.31	11.14	−0.32	−1.74
Ca	Ca^{2+}	$CaCO_3$, $CaMg(CO_3)_2$	290,500	259,500	460,000	131,000	114,000	97,100	64,000	0.74	0.42	0.012	0.010
Mg	Mg^{2+}	$CaMg(CO_3)_2$	7100	78,300	1,300,000	20,500	45,700	12,700	28,100	0.10	0.61	−0.01	0.01
Fe	Fe^{2+}	$Fe(OH)_3$, FeS_2	11,600	1500	132	6	63	5	5	0.00	0.00	0.00	0.00
Si	H_4SiO_4	SiO_2	57,800	38,500	28	16,830	8789	13,318	5514	0.51	0.25	0.01	0.00
Al	$Al(OH)^{4-}$	clay minerals	10,250	1900	21	3.7	2.9	2.0	2.0	0.00	0.00	0.00	0.00
As	AsO_4^{3-}	$Fe(OH)_3$	3.4	1.3	61.6	1.7	1.8	0.3	0.3	0.16	0.33	0.03	0.04
Ba	Ba^{2+}	$BaSO_4$, feldspar	76	8	8	83	70	51	8	1.50	1.45	0.04	0.78
Be	Be^{2+}	clay minerals	2.9	2.2	0.3	0.03	0.04	0.03	0.03	0.02	0.02	0.00	0.00
Co	Co^{2+}	FeS_2	3.4	0.7	0.5	0.11	0.05	0.03	0.03	0.02	0.06	0.00	0.01
Cr	CrO_4^{2-}	clay & heavy minerals	70	20	5.2	0.80	1.2	0.6	0.6	0.02	0.05	0.00	0.00
Cu	Cu^{2+}	clay & heavy minerals	19	2	12.5	2.5	2.1	0.9	0.9	0.11	0.77	0.01	0.09
Mo	MoO_4^{2-}	$Fe(OH)_3$, FeS_2	0.5	0.5	10.6	4.5	1.5	0.2	0.2	0.93	0.69	0.78	0.20
Ni	Ni^{2+}	FeS_2, $CaCO_3$	17.4	2.1	3.9	5.1	2.5	0.2	0.3	0.03	0.24	0.02	0.09
Pb	Pb^{2+}	$CaCO_3$ & clay minerals	2.1	1.8	0.5	0.3	0.3	0.3	0.3	0.31	0.29	0.00	0.00
Rb	Rb^{+}	clay minerals	5.0	2.4	124.9	2.7	2.9	1.0	0.5	0.44	0.36	0.02	0.01
Sr	Sr^{2+}	$CaCO_3$	649	148	7216	555	345	236	78	0.81	0.79	0.04	0.20
U	UO_2^{2+}	$Fe(OH)_3$	2.6	1.4	2.5	2.0	1.4	0.8	0.5	0.72	0.61	0.04	0.05
V	VO_4^{2-}	$Fe(OH)_3$	43.2	15.8	71.8	1.7	3.0	0.3	1.2	0.02	0.13	0.00	0.00
Zn	Zn^{2+}	clay & heavy minerals	35	7	19	117	146	3	4	0.21	1.05	0.28	2.92

(M)EF ≥ 0.01 = mobilization, *(M)EF* ≤ −0.01 = immobilization, and else = mobilization equilibrium. *MEF* is calculated for salinized groundwater, *EF* for BGC quality.
Concentrations of Au, Bi, Cd, Ce, Cs, Dy, Er, Eu, Ga, Gd, Hf, Hg, Ho, In, La, Lu, Nb, Nd, Pd, Pr, Pt, Re, Rh, Ru, Sb, Sm, Sn, Ta, Tb, Te, Th, Tl, Tm, Y, and Zr were <0.05 μg/L in salinized groundwater, and hence their behavior could not be established.
NB: A difference in the mobilization of some elements (e.g. V) may arise when utilizing ancient clean seawater (e.g. > 40 years ago). This is due to slightly different concentrations of some major and trace elements (see Table S6, *Supplementary Material*).
[a] Baseline Groundwater Concentration (BGC) derived by Khadra and Stuyfzand (2014).

Table 5
Hydrochemistry of intruding seawater and initial ambient groundwater used in PHREEQC-2 modeling along path 1 (limestone) and path 2 (dolomitic limestone); ions in mmol/L.

		Ca	Mg	Na	K	HCO_3	Cl	SO_4	pH
Mediterranean Sea water		11.5	53.5	505	12.0	2.7	575	33.3	7.93
Onshore groundwater	path 1	3.0	0.5	1.1	0.1	5.4	1.4	0.6	6.89
	path 2	4.9	0.7	2.8	0.1	5.4	5.0	1.1	6.68

1987). All major and trace elements are assessed here for calcareous salinized samples in the limestone (C_6-Q) and dolomitic limestone (C_{4c}-C_5) hosting units. The aim is to define: (1) the affinity of these elements toward (im)mobilization, and (2) the associated difference in mobilization degree between limestone and dolomitic limestone. This is done by calculating their Mixing Enrichment Factor (*MEF*) via Eq. (10) (Table 4). Also listed are the predominant ionic forms in (sub)oxic environment, and the main aquifer sources/sinks.

MEF values of the major and trace elements including those statistically interlinked to SWI show the following results:

1. Ca is mobilized by salinization, Na and K are immobilized, and Fe maintains an equilibrium status. This applies to both limestone and dolomitic limestone, but with higher immobilization of Na and K in the latter.
2. Mg is immobilized for the limestone groundwater but mobilized for the dolomitic limestone.
3. Si is mobilized in the limestone unit only.
4. As, Ba, Cu, Ni, Rb, Sr, U and Zn are mobilized in both domains.
5. As, Mo, Rb and U show relatively higher mobilization in the salinized limestone unit.
6. Al, Be, Co, Cr, Pb and V reveal no affinity to mobilize due to SWI, and hence their slight increase in groundwater reflects admixing with seawater.

35 more TEs with <0.05 μg/L in all groundwater samples could not be evaluated on their behavior (Table 4). Some of them like Ce, Nb, Nd, Y and Zr have significant levels in the hosting rocks (median is 1–50 ppm) (Table 3), but reveal concentration levels below detection in all water samples. This is in harmony with their very weak mobilization potential at near pH neutral conditions (Janssen and Verweij, 2003).

3.5. Flow path reactive transport modeling results

Reactive transport simulations were performed along two flow paths following presumed saltwater intrusion lines: flow path 1

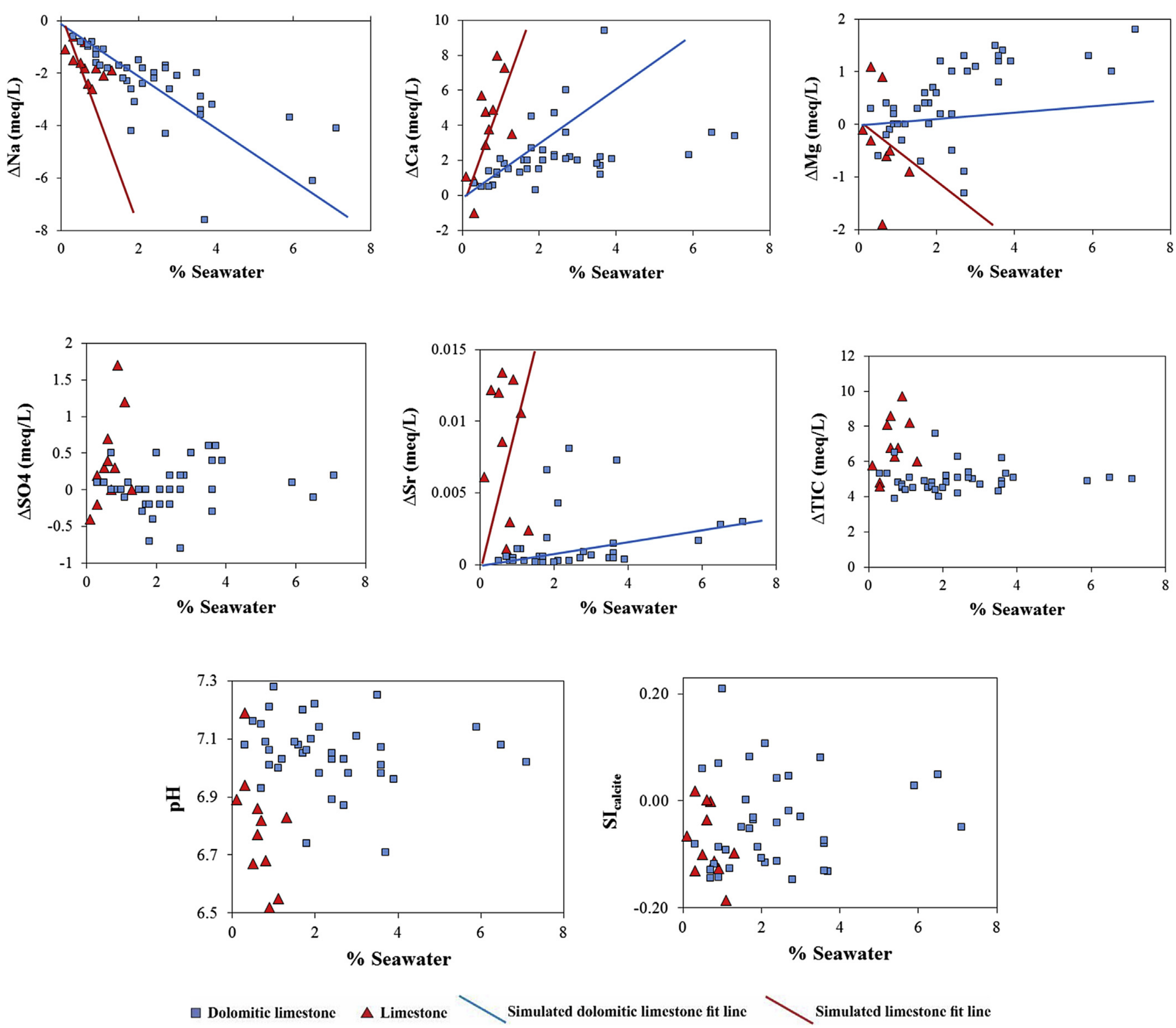

Fig. 3. Ionic deltas (Δ) of Na, Ca, Mg, SO_4, Sr and TIC, pH and $SI_{calcite}$ vs. % of seawater. Samples are discerned based on formations from which they derive, the C_{4c}-C_5 aquifer (dolomitic limestone), and the C_6-Q units (limestone). The simulated (solid) lines are generated via PHREEQC (see "*Flow path reactive transport modeling results*" section).

Table 6
PHREEQC-2 forward dual porosity modeling physical and geochemical parameters. L.S = limestone; Dol. L.S = dolomitic limestone.

Flow path	L (m)	Δt (year)	Δx (m)	# of transport steps	# cells	ε_m	ε_{im}	v (m/d)	α_L (m)
1	1200	2.7e-01	10	33	241	0.008	0.08	0.10	11
2	1500	2.3e-01	5	40	601	0.03	0.12	0.06	30

Flow path	CEC (mol/kg H_2O)		Rock density (kg/L)		Mole fractions $Ca_{(x)}Mg_{(y)}Sr_{(z)}CO3$		
	mobile cells	immobile cells	L.S	Dol. L.S	Ca	Mg	Sr
1	0.005	0.1	2.70	–	1.00	0.00	0.0018
2	0.005	0.02	–	2.85	0.75	0.25	0.0003

ε_m values were fine-tuned to get a reasonable description of the observed ΔNa, ΔCa, ΔMg and ΔSr patterns (Fig. 3).
ε_{im} relied on literature values.

across the cultivation strip of the Damour village in the coastal plain via the C_6 limestone unit, and flow path 2 across the Naameh-Haret El Naameh villages (an area heavily stressed by groundwater abstraction) in the dolomitic limestone aquifer (C_{4c}-C_5) (see Figs. 1 and 2). Flowlines start with the Mediterranean Sea water offshore, and invade the coast initially filled with the average groundwater composition (fresh-brackish) as recorded in 2002. The simulations are then allowed to run for 9 years to generate the year 2011 conditions. The chemistry of ambient groundwater and intruded seawater is provided in Table 5; physical and geochemical PHREEQC-2 parameters are provided in Table 6. Simulations involved ideal intrusion assuming uniform pumping in wells along the two flow paths (Fig. 1) although in reality non-uniform extraction may produce irregular patterns where salinity may rise and fall before it stabilizes with fresh-brackish water.

The literature lacks data describing Cation Exchange Capacity (*CEC*) in karstified limestone and dolomitic limestone. The *CEC* of rocks in meq/kg is estimated here as 7 × % clay +35 × % organic carbon (Appelo and Postma, 2005). This equation may apply for the bulk rock; however, the effective *CEC* is expected to be lower especially for the mobile (fractured) sections of the dual porosity medium. Therefore, immobile and mobile cells were assigned different values in the 1-D dual domain reactive transport model. The initial values of CEC_{immobile} (23–65 meq/kg) relying on clay and organic carbon content were in reasonable agreement with the scarce literature on limestone (e.g. Gillespie et al., 2001; Ertas and Topal, 2008) and dolomitic limestone (e.g. Gillespie et al., 2001; Topal and Kaya, 2016), as obtained in the lab for rock samples. The CEC_{mobile} was initially assigned one order of magnitude lower than CEC_{immobile}. Due to higher porosity, *CEC* is higher in the matrix than in the mobile domain as it is expressed in meq/L (i.e. the porosity difference sets the *CEC* difference between mobile and immobile). In addition, concentrated and sometimes turbulent flow in the mobile zones (fissures, large diameter solution channels) may reduce the *CEC* due to polishing effects (reducing surface area), and perhaps by selective erosion of fines and more oxidation of organic material. Later both *CEC*s were fine-tuned to lower values by model optimization supported by sensitivity analysis in order to better represent actual *CEC*s in the natural environment.

Applying a 1-D dual porosity formulation, both mobile and stagnant zones were initially filled with fresh-brackish water. Later the seawater was allowed to intrude through advection along the selected flow paths. A constant inland groundwater velocity was assumed, estimated at 0.10 m/d along path 1 based on available hydraulic head and aquifer conductivity data, and 0.06 m/d for flow path 2, as deduced from the landward movement of the 250 mg/L chloride isoline between 2002 (Khadra, 2003) and 2011 (Khadra and Stuyfzand, 2014). Dispersivity was estimated based on Eq. (13), and then fine-tuned during the calibration process where necessary. Molecular diffusion could be neglected.

The *wateq4f.dat* database was used in PHREEQC-2 simulations to account for Mg-calcite, which is thermodynamically treated as a calcite-magnesite solid solution. This is applied to path 2 only via the dolomitic limestone aquifer. Moles of calcite and magnesite were deduced from the hosting rocks geochemistry (Table 3). Activity coefficients and mole fractions (Table 6) were used to calculate the dimensional Guggenheim parameters necessary to determine the activities of components in a non-ideal binary solid solution (Glynn and Reardon, 1990). Pure $SrCO_3$ was also allowed to equilibrate with aqueous solution for both flow paths. The *CEC* estimated in meq/kg was converted into mol/kg of water as required for PHREEQC calculations. Sensitivity analysis (with 2 times lower/higher values) was performed to check the impact of CEC_{immobile} on the response of major ions. It confirmed the minor impact of CEC_{mobile} (Fig. S2 and S3, *Supplementary Material*). The model was capable to generate: (1) a reasonable description of the observed ΔNa, ΔCa, ΔMg and ΔSr patterns (Fig. 3), and (2) a close match between simulated and observed concentrations in wells along the two flow paths (Fig. 4). The results of simulation runs without cation exchange are also added to the same plots to show the significance of this process. Fig. 4a shows clear differences even for the closest observation whereas Fig. 4b generally shows less changes.

The 1-D transport model along flow path 1 (via the C_6 limestone unit) over a 9-year period (from 2002 to 2011) shows Ca surplus (43 meq/L), and simultaneous Na, Mg and K deficit (Figs. 4a and 5a). This pattern is typical for cation exchange during salinization. At the shoreline, the intruding Mediterranean Sea water (Table 5), supersaturated with respect to $CaCO_3$, induces calcite precipitation by desorbing Ca, and at ca. 35 m calcite dissolves (Fig. 6a). This dissolution is probably driven by the mixing of freshwater and saltwater, which leads to undersaturation. It tends to concentrate at the freshwater side of the mixing zone or near the saline side at the discharge areas (Rezaei et al., 2005). Sr shows a similar response to Ca along this flow path; however, the strontium maturity index (Khadra and Stuyfzand, 2014) pleads for no coprecipitation of Sr with $CaCO_3$. The decrease is therefore attributed to Sr sorption on exchange surfaces, being more in the limestone unit.

Flow path 2 (dolomitic limestone) (Fig. 4b) shows three features which are clearly different from flow path limestone: (i) the peak of Ca surplus at the start of the intrusion zone; (ii) Mg being the key counter cation (whilst it is Na at flow path limestone), and (iii) a nearly suppressed response of Sr. The model simulates the formation of calcite-magnesite solid solution (Fig. 6b) as induced by the high Mg:Ca ratio of intruding seawater (see Table S1 for Mg:Ca ratios in seawater and fresh water) according to the following reaction:

$$Ca_xMg_{(1\text{-}x)}CO_3 + yMg^{2+} \rightarrow Ca_{x\text{-}y}Mg_{(1\text{-}x+y)}CO_3 + yCa^{2+}$$

As a result, Ca is added while Mg is removed from groundwater. This mineral-water interaction process intensifies the impact of

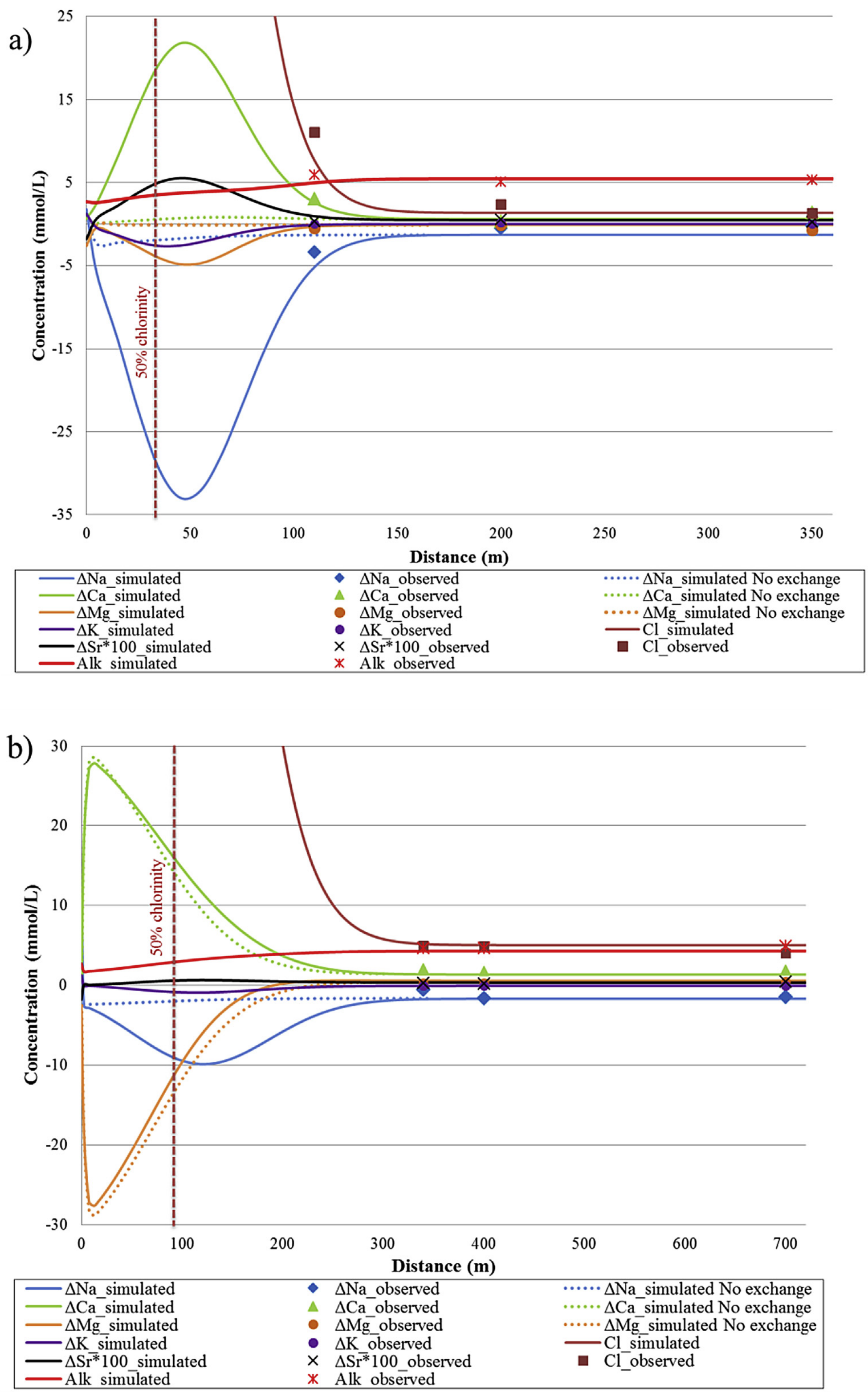

Fig. 4. 1-D dual porosity flow path simulations of the current (2011) conditions of advective transport of seawater along (a) path 1 into the C6 unit (limestone), and along (b) path 2 into the C4c-C5 unit (dolomitic limestone). Path 2 considers a calcite-magnesite solid solution. Stagnant zones are modeled using first-order exchange approximations assuming dual-porosity medium. Negative values = depletion, positive values = enrichment; ΔNa, ΔCa, ΔMg, ΔK and ΔSr are calculated via Eq. (4). Vertical dashed red line is the 50% breakthrough point of seawater chlorinity. Dot-dashed lines show simulation results without cation exchange. (For interpretation of the references to colour in this figure legend, the reader is referred to the web version of this article.)

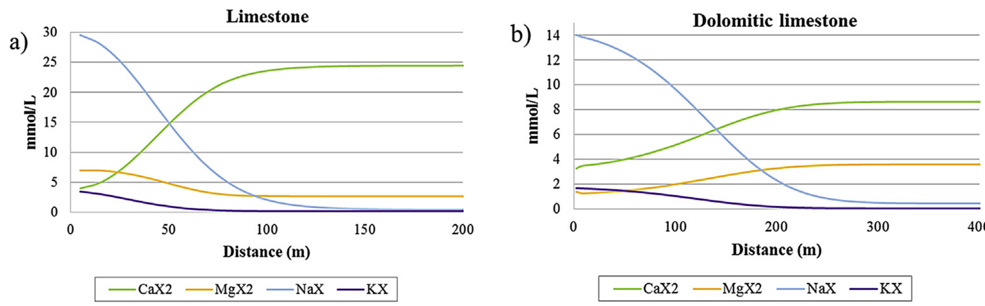

Fig. 5. 1-D dual porosity flow path simulations of the replacement of Na, Mg, Ca and K on the cation exchanger along (a) path 1 (limestone), and (b) path 2 (dolomitic limestone). Path 2 considers a calcite-magnesite solid solution.

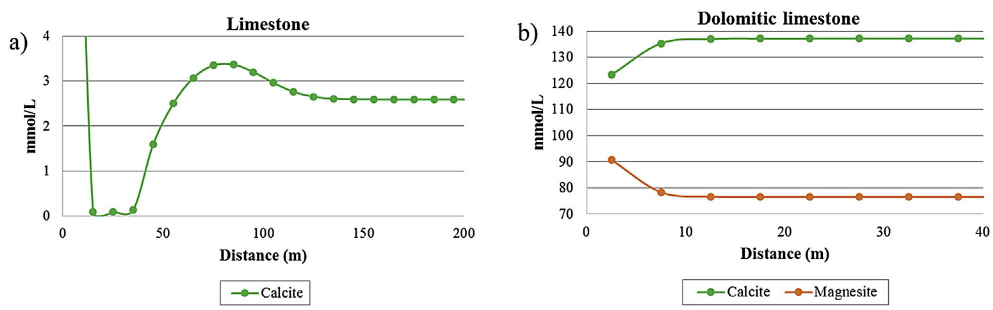

Fig. 6. 1-D dual porosity flow path simulations of calcite and magnesite along (a) path 1 (limestone), and (b) path 2 (dolomitic limestone), showing the spatial changes in the solid phase (e.g. the change of Ca in calcite and Mg in magnesite). Path 2 considers a calcite-magnesite solid solution.

cation-exchange (Ca surplus vs. Mg deficit) along flow path dolomitic limestone. Note that the Mg deficit induces Mg desorption, and causes a lower fraction of the exchangeable Mg in the salinized zone compared to the fresh water zone, whereas this situation is opposite at flow path limestone (Fig. 5). Noteworthy to mention that path 1 shows a shorter exchange zone although it has higher *CEC*. This is because the groundwater flow velocity along path 1 is 1.6 times higher than along path 2.

4. Discussion

4.1. Hydrogeochemical disparities

The discussion here focuses on major hydrogeochemical differences between limestone and dolomitic limestone units in accordance to: (a) geochemical activity, and (b) salinity effects. This includes the main geochemical processes, and the response of major chemical constituents and trace elements in the salinized groundwater.

4.1.1. Main geochemical processes

The main discerned geochemical processes in the studied aquifers are carbonate ($Ca_xMg_ySr_zCO_3$) dissolution/precipitation, and typical cation exchange reactions in the saltwater mixing zone. The primary hydrochemical difference between samples from limestone and dolomitic limestone consists of the contrasting ratios of Ca:Mg and Ca:Sr, for both the aquifer rock and water samples. Salinization of groundwater in the limestone coastal plain leads to more Ca mobilization compared to the dolomitic limestone. This is evidenced by a higher positive ΔCa (average ΔCa = 10.5 and 4.6 meq/L) (Fig. 3) and *MEF* values (0.012‰ and 0.010‰) (Table 4) for the limestone and dolomitic limestone, respectively. Carbonate dissolution and cation exchange both contribute to the recorded mobilization. This is due to more Ca in the limestone hosting unit (36.3 wt.%) and probably its adsorption complex than in the dolomitic limestone (24.5 wt.%), in addition to higher pCO_2 characterizing the coastal plain region compared to the dolomitic limestone with less vegetation and a higher altitude of the recharge area.

On the other hand, seawater intrusion triggers a further Ca substitution by Mg of the dolomitic limestone, or the precipitation of a more dolomitic limestone, driven by the high Mg concentration compared to Ca, in the intruding seawater. Dolomitization or high Mg-calcite precipitation has been observed elsewhere with different Mg:Ca molar ratios (e.g. Whitaker and Smart, 1993; Sacks and Tihansky, 1996). This response at high salinity in the dolomitic limestone overwhelms cation exchange unlike the limestone unit where pure calcite precipitation/dissolution is stimulated by Na/Ca exchange and mixing of two water bodies with different pCO_2, respectively. Under fresh-brackish water conditions, Mg is released to solution in the dolomitic limestone (*MEF* = 0.01‰) exchanging (besides Ca) with Na and K. This behavior is different for the limestone where Mg (*MEF* = −0.01‰), Na and K exchange for Ca.

The data also reveals higher mobilization of Sr under freshwater conditions in the limestone unit (Table 4), which is attributed to more incorporation of Sr into $CaCO_3$. However, the *MEF* scores, contrary to the 1-D reactive transport model, indicate that SWI stimulates higher mobilization in the dolomitic limestone despite Sr lower concentrations in the hosting rocks, a difference not easy to explain.

Silica (quartz or opal) dissolution with slightly higher mobilization in the limestone unit, is probably due to more silica weathering from the overlying quaternary (Q) sand. The zero *MEF* data for Fe indicate that reactions such as pyrite oxidation or reductive iron hydroxide dissolution do not take place, as expected.

4.1.2. Behavior of trace elements

Based on statistical variances and the enrichment factors, the response of 15 TE to SWI, and to geochemical contrast between limestone vs. Dolomitic limestone shows the following traits:

1 TEs in fresh groundwater: limestone versus dolomitic limestone

The concentrations of Ba, Rb, Sr and U in fresh groundwater are significantly higher in limestone than in dolomitic limestone, which is in line with their differences in geochemistry (Table 4). On the other hand, significant differences in geochemistry between both units (limestone higher), are not reflected in differences in the concentrations of Al, As, Co, Cr, Cu, Ni and Zn in natural background groundwater (Table 4). Only V shows a reverse trend, notwithstanding lower contents of dolomitic limestone, the concentration in its groundwater is higher.

It can therefore be concluded that Ba, Rb, Sr and U are relatively mobile in limestone and are probably dissolving from it, whereas the other TEs are not. *EFs* for the background groundwater qualities of both units (Table 4) show immobilization for Al, Co and Cr, which matches their insoluble behavior in neutral water (Fishbein, 1981; Edmunds and Smedley, 1996; Drever, 1997). As, Cu, Ni and Zn however are more mobilized in the dolomitic limestone as indicated by their higher *EF* values. (Hydro)oxides sorption surfaces explain this discrepancy because they form the main substrates for adsorption, and they are less dominant in the dolomitic limestone unit.

Previous studies on trace element enrichment in (dolomitic) limestone aquifers are scarce. Frondini et al., 2014, observed in the Sassolungo and Sella dolomite aquifer in Italy that Ba, Sr and U, and to a smaller extent Rb were enriched in its groundwater, which is in line with this study.

2 TEs in salinized groundwater: limestone versus dolomitic limestone

Concentrations of As, Ba, Cu, Ni, Rb, Sr and U increase by SWI in both units. It is likely that the higher salinity stimulates both their desorption (through a higher expelling power) and the dissolution of hosting minerals (through the higher ionic strength reducing the activity coefficients and increasing ion complexation). In addition, part of the mobilization could be attributed to the lower pH induced by salinity (see salinized groundwater in Table S1; *Supplementary Material*), since the higher Ca (due to Na/Ca exchange) eventually leads to $CaCO_3$ precipitation.

As and U reveal more mobilization in the limestone unit whereas the others are more enhanced in the dolomitic limestone (Table 4). As and Ni are mobilized although they occur at low levels in natural background water (<0.4 μg/L) (Table 4). This behavior of arsenic, contrary to observations in fresh groundwater, is attributed to arsenate species initially adsorbing on oxyhydroxides at neutral pH (Drever, 1997), but SWI later facilitates more mobilization. SWI also stimulates Ba and Sr mobilization either by cation exchange or dissolution from carbonate rocks (Sr) and barite or feldspars (Ba). The positive correlation of As, Ba and Sr with seawater intrusion has been observed in other aquifers as well (e.g. Mondal et al., 2010; Stuyfzand and Mendizabal, 2010). *MEF* scores reveal higher mobilization of Ba and Sr in the salinized dolomitic limestone aquifer despite their lower concentrations in the hosting aquifers.

The observed differences in the behavior of Cu, Ni, Rb and U between the two units is justified by the same reasoning of their recorded discrepancies in freshwater.

3 TEs independent of salinity and (dolomitic) limestone geochemical contrast

Al, Be, Co, Cr, Pb and V show no significant signs of (im) mobilization ($-0.01 \leq MEF \leq 0.01$) for both limestone and dolomitic limestone, independently of salinity. This response is attributed to their insoluble behavior in neutral and alkaline pH conditions (Fishbein, 1981; Edmunds and Smedley, 1996; Drever, 1997) in addition to the high affinity of Be (WHO, 2001), Pb (Hem, 1992) and V (Luengo-Oroz et al., 2014) to adsorb on sediment surfaces. V is statistically interlinked to SWI in both units, but its relationship with intruding seawater is not clear due to the big contrast between recent and ancient seawater.

Statistical analyses also show that Mo and Zn are independent of salinity and (dolomitic) limestone geochemical contrast. However, their *MEF* scores reveal high mobilization in both units. This contradicts the Mo immobilization observed in salinizing anoxic sandy aquifers (Stuyfzand, 1993b). Mo is known to mobilize in anoxic environments where reductive Fe dissolution controls Mo release to the aqueous solution (Bennett and Dudas, 2003; Smedley et al., 2014; Pichler and Mozaffari, 2015). However, this scenario is irrelevant here due to dominance of oxidizing conditions. In fact, Mo levels record a progressive increase down the flow gradient. In this case, the mobilization of Mo may be attributed to alkaline pH conditions and subsequent desorption from Mo-rich minerals (e.g. Fe or Al oxides). This response is due to low retention of Mo on solid surfaces at pH > 5 (Goldberg and Forster, 1998; Carroll et al., 2006), and a function of groundwater residence time (Smedley et al., 2014). A similar behavior has been observed elsewhere (e.g. Smedley and Edmunds, 2002). The higher Fe and Al content of the limestone hosting unit (Tables 3 and 4) explains its higher Mo mobilization compared to the dolomitic limestone.

The behavior of Zn could be related to bias due to its corrosion from wells with old galvanized iron pipes. Low levels of Pb in groundwater supports this hypothesis because of its affinity to adsorb on iron and form lead-iron scales (HDR, 2009).

4.2. TEs permissible levels

TEs in groundwater normally occur at very low concentrations. They are harmful only when permissible levels are exceeded. In general, two main natural causes potentially raise TEs in coastal groundwaters: (1) water-rock interactions, and (2) saltwater intrusion. The latter has more versatile effect due to direct seawater mixing or enhanced mobilization. In this study, the collected data shows that TEs have increased by few μg/L only. All TEs including heavy metals (e.g. copper, lead and zinc) are still below permissible drinking water levels in accordance to the best recognized standards (EU, 1998; US EPA, 2008; WHO, 2008) (Table S7, *Supplementary Material*). They reveal satisfactory results even for the brackish water samples. Hence, it is obvious that the dissolution of (dolomitic) limestone carbonate rocks contributes very little to TEs in groundwater (Sr excluded, but there are no quality standards for Sr), and the impact of moderate SWI is not as bad as for some main constituents (e.g. Na, Cl and Ca). In the study area, TEs pose no health concern to date, but progressive salinization may soon lead to unfavorable shifts.

5. Conclusions

Four lines of research were followed in this paper to assess water quality differences between limestone and dolomitic limestone aquifers disturbed by saltwater intrusion (SWI) in coastal areas. These included: (1) nonparametric statistical tests on 4 water groups (limestone and dolomitic limestone with and without salinization); (2) ionic shifts of major chemical constituents from ideal freshwater-seawater mixing; (3) a new parameter called Mixing Enrichment Factor (*MEF*) to assess the (im)mobilization of trace elements (TEs) and main constituents under mixing conditions;

and (4) 1-D dual porosity flow path PHREEQC reactive transport simulations. This multiple approach was applied to a moderately salinizing coastal aquifer system in Lebanon (Eastern Mediterranean) where main hydrochemical disparities between limestone and dolomitic limestone were revealed. The discussion focused on 8 major chemical constituents (Na, K, Ca, Mg, SO_4, TIC, Fe and Si), and 15 trace elements (Al, As, Ba, Be, Co, Cr, Cu, Mo, Ni, Pb, Rb, Sr, U, V and Zn). 35 other TEs were analyzed, but were excluded from the comparison because of very low concentrations (<0.05 μg/L). Some of them like Ce, Nb, Nd, Y, and Zr had significant levels in the hosting rocks (1–50 ppm), but remained below detection in the salinized water samples preventing final conclusions about any (im)mobilization.

Two main chemical processes explained the non-conservative behavior of the major constituents in both limestone and dolomitic limestone units. These are the dissolution of $Ca_xMg_ySr_zCO_3$ and cation exchange spurred by saltwater intrusion. The dolomitic limestone unit showed less carbonate dissolution due to a lower unsaturated zone pCO_2 connected with less vegetation and a higher altitude of the recharge area, and a lower cation exchange capacity compared to limestone. The presence of high Mg-calcite raised the Mg levels in groundwater, and enhanced the Mg participation (besides Ca) in the exchange for Na and K. Fe revealed no difference between the two aquifers. Silica (quartz or opal) showed more mobilization in the limestone unit, which is probably dictated by more dissolution in the overlying quaternary sand-rich unit, and therefore does not contribute to the geochemical contrast between both aquifers.

As, Ba, Cu, Ni, Rb, Sr and U revealed the strongest mobilization among the investigated TEs during saltwater intrusion under calcareous (sub)oxic conditions. Zn is presumably biased by corrosion of well materials, and the apparent Mo mobilization is independent of SWI and (dolomitic) limestone geochemical contrast.

Besides the stimulating role of SWI, the geochemical contrast between limestone and dolomitic limestone proved to be an important factor explaining part of the observed variation in the concentration of TEs in fresh groundwater. For example, As, Cu and Ni recorded stronger mobilization in the freshwater dolomitic limestone, whereas Ba, Rb, Sr and U were more mobilized in the limestone unit. Other elements like Al, Be, Co, Cr, Pb and V showed no (im)mobilization in either rock type. The observed TE discrepancy between the limestone and dolomitic limestone units is geochemically mainly linked to the higher Sr content of limestone and its higher content of clay minerals and iron (hydro)oxides in the limestone unit.

To conclude, it was demonstrated that: (1) the geochemical contrast between the limestone and dolomitic limestone aquifers do have an effect on the behavior of some major constituents and TEs, (2) carbonate rocks do not form a significant geogenic sources of TEs (Sr excluded), (3) the mobilization of TEs by salinization is small compared to the enhanced concentration rise produced by direct seawater mixing, and (4) the current TEs levels in the studied aquifer are far below the drinking water limits, thanks to a moderate salinization to date. Their current levels pose no concern nowadays, a situation that should not be taken for granted if excessive pumping persists.

Acknowledgements

Prof. Dr. Thomas Pichler and one anonymous reviewer are highly appreciated for their constructive comments and suggestions that helped to improve this manuscript. We would like also to thank agricultural engineer Mr. Khaled Aoun for his continuous aid in data gathering. The unlimited cooperation of Mr. Abed El-Hadi Mezher, from the municipality of Naameh, is acknowledged as well. This research did not receive any specific grant from funding agencies in the public, commercial, or not-for-profit sectors.

Appendix A. Supplementary data

Supplementary data related to this article can be found at http://dx.doi.org/10.1016/j.apgeochem.2017.02.005.

References

Al Kuisi, M., Abed, A.M., Mashal, K., Saffarini, G., Saqhour, F., 2015. Hydrogeochemistry of groundwater from karstic limestone aquifer highlighting arsenic contamination: case study from Jordan. Arab. J. Geosci. 8, 9699–9720. http://dx.doi.org/10.1007/s12517-015-1919-z.

Appelo, C.A.J., 1994. Cation and proton exchange, pH variations, and carbonate reactions in a freshening aquifer. Water Resour. Res. 30 (10), 2793–2805.

Appelo, C.A.J., Postma, D., 2005. Geochemistry, Groundwater and Pollution, second ed. Balkema Publishers, the Netherlands.

Arkadan, A., 1999. The Geology, Geomorphology and Hydrogeology of the Damour-Awali Area Coastal and Hinterland. M.S. Thesis. American University of Beirut, Lebanon.

Arkadan, A., 2008. Climatic changes in Lebanon, predicting uncertain precipitation events — do climatic cycles exist? In: Zereini, F., Hötzl, H. (Eds.), Climatic Changes and Water Resources in the Middle East and North Africa, Environmental Science and Engineering. Springer, Berlin Heidelberg, pp. 59–74.

Ayotte, J.D., Szabo, Z., Focazio, M.J., Eberts, S.M., 2011. Effects of human-induced alteration of groundwater flow on concentrations of naturally-occurring trace elements at water-supply wells. Appl. Geochem 26, 747–762. http://dx.doi.org/10.1016/j.apgeochem.2011.01.033.

Ben Ammar, S., Taupin, J.D., Zouari, K., Khouatmia, M., 2016. Identifying recharge and salinization sources of groundwater in the Oussja Ghar el Melah plain (northeast Tunisia) using geochemical tools and environmental isotopes. Environ. Earth Sci. 75, 606. http://dx.doi.org/10.1007/s12665-016-5431-x.

Bennett, B., Dudas, M.J., 2003. Release of arsenic and molybdenum by reductive dissolution of iron oxides in a soil with enriched levels of native arsenic. J. Environ. Eng. Sci. 2, 265–272. http://dx.doi.org/10.1139/s03-028.

Bouderbala, A., Remini, B., Saaed, Hamoudi A., Pulido-Bosch, A., 2016. Application of multivariate statistical techniques for characterization of groundwater quality in the coastal aquifer of Nador, Tipaza (Algeria). Acta Geophys. 64 (3), 670–693. http://dx.doi.org/10.1515/acgeo-2016-0027.

Bradford, S.A., Kim, H., 2010. Implications of cation exchange on clay release and colloid-Facilitated transport in porous media. J. Environ. Qual. 39, 2040–2046. http://dx.doi.org/10.2134/jeq2010.0156.

Brook, G.A., Folkoff, M.E., Box, E.O., 1983. A world model of soil carbon dioxide. Earth Surf. Proc. 8, 79–88.

Carroll, K.C., Artiola, J.F., Brusseau, M.L., 2006. Transport of molybdenum in a biosolid-amended alkaline soil. Chemosphere 65, 778–785. http://dx.doi.org/10.1016/j.chemosphere.2006.03.044.

Dai, Z., Samper, J., Ritzi Jr., R., 2006. Identifying geochemical processes by inverse modeling of multicomponent reactive transport in the Aquia aquifer. Geosphere 2 (4), 210–219. http://dx.doi.org/10.1130/GES00021.1.

de Montety, V., Radakovitch, O., Vallet-Coulomb, C., Blavoux, B., Hermitte, D., Valles, V., 2008. Origin of groundwater salinity and hydrogeochemical processes in a confined coastal aquifer: case of the Rhône delta (Southern France). Appl. Geochem 23, 2337–2349. http://dx.doi.org/10.1016/j.apgeochem.2008.03.011.

Drever, J., 1997. The Geochemistry of Natural Waters, third ed. Prentice Hall, New Jersey, p. 436.

Dubertret, L., 1955. Carte Géologique du Liban au 1/200000 avec notice explicative. République Libanaise. Ministère des Travaux Publiques, Beirut, Lebanon.

Edmunds, W.M., Smedley, P.L., 1996. Groundwater geochemistry and health: an overview. In: Appleton, et al. (Eds.), Environmental Geochemistry and Health: with Special Reference to Developing Countries. Geological Society of London Special Publication, London no.113, 91–105.

Einsiedl, F., Maloszewski, P., Stichler, W., 2009. Multiple isotope approach to the determination of the natural attenuation potential of a high-alpine karst system. J. Hydrol. 365, 113–121. http://dx.doi.org/10.1016/j.jhydrol.2008.11.042.

El-Fadel M., Rachid G., Alameddine I., Abu Najm M., 2014. Saltwater Intrusion in karst aquifers along the Eastern Mediterranean. 23rd Salt Water Intrusion Meeting, June 16-20, Husum, Germany, pp. 311–314.

Emblanch, C., Fidelibus, M.D., Futo, I., Hertelendi, E., Lambrakis, N., Vengosh, A., Zojer, H., Zuppi, G.M., 2005. Environmental tracing methods. In: Tulipano, et al. (Eds.), Groundwater Management of Coastal Karstic Aquifers, COST Action 621, Final Report, EUR 21366. COST Office, Luxemburg.

Ertas, T., Topal, T., 2008. Quality and durability assessments of the armourstones for two rubble mound breakwaters (Mersin, Turkey). Environ. Geol. 53, 1235–1247. http://dx.doi.org/10.1007/s00254-007-0712-z.

EU, 1998. Council directive 98/83/EC of 3 November 1998 on the quality of water intended for human consumption. Official J. Eur. Communities L 330/32. 32–54.

Faimon, J., Ličbinska, M., Zajiček, P., Sracek, O., 2012. Partial pressures of CO_2 in

epikarst zone deduced from hydrogeochemistry of permanent drips, the Moravian karst, Czech Republic. Acta Carsologica 41 (1), 47–57.
Fidelibus, M.D., 2003. Environmental tracing in coastal aquifers: old problems and new solutions. In: Coastal Aquifers Intrusion Technology. Mediterranean Countries. Publ. IGME, Madrid, pp. 9–111.
Fidelibus, M.D., Giménez, E., Morell, I., Tulipano, L., 1993. Salinization processes in the Castellon Plain aquifer (Spain). Study and modelling of saltwater intrusion into aquifers. Proceedings 12th Saltwater Intrusion Meeting, CIMNE, Barcelona pp. 267–283.
Fiket, Ž., Rožmarić, M., Krmpotić, M., Benedik, L., 2015. Levels of major and trace elements, including rare earth elements, and ^{238}U in Croatian tap waters. Environ. Sci. Pollut. Res. 22, 6789–6799. http://dx.doi.org/10.1007/s11356-014-3869-5.
Fishbein, L., 1981. Sources, transport and alterations of metal compounds: An overview. I. Arsenic, Beryllium, cadmium, chromium, and Nickel. Environ. Health Perspect. 40, 43–64.
Frondini, F., Zucchini, A., Comodi, P., 2014. Water–rock interactions and trace elements distribution in dolomite aquifers: the Sassolungo and Sella systems (Northern Italy). Geochem. J. 48, 231–246. http://dx.doi.org/10.2343/geochemj.2.0301.
Gillespie, M.R., Kemp, S.J., Vickers, B.P., Waters, C., Gowing, C.J., 2001. Cation-exchange Capacity (CEC) of Selected Lithologies from England, Wales and Scotland. Environment Agency R&D Technical Report P2–222/TR. British Geological Survey, Keyworth, Nottingham.
Glynn, P.D., Reardon, E.J., 1990. Solid-solution aqueous-solution equilibria—thermodynamic theory and representation. Am. J. Sci. 290, 164–201.
Goldberg, S., Forster, H.S., 1998. Factors affecting molybdenum adsorption by soils and minerals. Soil Sci. 163, 109–114.
Gonneea, M.E., Charette, M.A., Liu, Q., Herrera-Silveira, J.A., Morales-Ojeda, S.M., 2014. Trace element geochemistry of groundwater in a karst subterranean estuary (Yucatan Peninsula, Mexico). Geochimica Cosmochimica Acta 132, 31–49. http://dx.doi.org/10.1016/j.gca.2014.01.037.
Habtemichael, Y.T., Fuentes, H.R., 2016. Hydrogeochemical analysis of processes through modeling of seawater intrusion impacts in Biscayne aquifer water quality, USA. Aquat. Geochem 1–13. http://dx.doi.org/10.1007/s10498-016-9287-1.
HDR, 2009. An Analysis of the Correlation between Lead Released from Galvanized Iron Piping and the Contents of Lead in Drinking Water. HDR Engineering Inc., Washington.
Heathcote, J.A., 1985. Carbonate chemistry of recent chalk groundwater in a part of East-Anglia, UK. J. Hydrol. 78, 215–227.
Hem, J.D., 1992. Study and Interpretation of the Chemical Characteristics of Natural Water. U.S. Geological Survey. Water Supply Paper 2254.
Herman, J., Back, W., Pomar, L., 1985. Geochemistry of groundwater in the mixing zone along the east coast of Mallorca, Spain. Karst Water Resources, Proceedings of the Ankara - Antalya Symposium. IAHS 161, 467–479.
Hinkle, D.E., Wiersma, W., Jurs, S.G., 2003. Applied Statistics for the Behavior Sciences. Houghton Mifflin Company, New York.
Janssen, R.P., Verweij, W., 2003. Geochemistry of some rare earth elements in groundwater, Vierlingsbeek, The Netherlands. Water Res. 37, 1320–1350. http://dx.doi.org/10.1016/S0043-1354(02)00492-X.
Khadra, W.M., 2003. Hydrogeology of the Damour-Upper Sannine-maameltain Aquifer. M.S. Thesis. American University of Beirut, Lebanon.
Khadra, W.M., Stuyfzand, P.J., 2014. Separating baseline conditions from anthropogenic impacts: example of the Damour coastal aquifer (Lebanon). Hydrol. Sci. J. 59, 1872–1893. http://dx.doi.org/10.1080/02626667.2013.841912.
Koh, D.-C., Chae, G.-T., Ryu, J.-S., Lee, S.-G., Ko, K.-S., 2016. Occurrence and mobility of major and trace elements in groundwater from pristine volcanic aquifers in Jeju Island, Korea. Appl. Geochem 65, 87–102. http://dx.doi.org/10.1016/j.apgeochem.2015.11.004.
Korfali, S., Jurdi, M., 2007. Assessment of domestic water quality: case study, Beirut, Lebanon. Environ. Monit. Assess. 135, 241–251. http://dx.doi.org/10.1007/s10661-007-9646-x.
Korfali, S., Jurdi, M., 2009. Provision of safe domestic water for the promotion and protection of public health: a case study of the city of Beirut, Lebanon. Environ. Geochem. Health 31, 283–295. http://dx.doi.org/10.1007/s10653-008-9218-1.
Langmuir, D., 1997. Aqueous Environmental Geochemistry. Prentice Hall, New Jersey.
Lin, C.Y., Musta, B., Abdullah, M.H., 2013. Geochemical processes, evidence and thermodynamic behavior of dissolved and precipitated carbonate minerals in a modern seawater/freshwater mixing zone of a small tropical island. Appl. Geochem 29, 13–31. http://dx.doi.org/10.1016/j.apgeochem.2012.10.029.
Lipson, D.S., McCray, J.E., Thyne, G.D., 2007. Using PHREEQC to simulate solute transport in fractured bedrock. Ground Water 45 (4), 468–472. http://dx.doi.org/10.1111/j.1745-6584.2007.00318.x.
Luengo-Oroz, N., Bellomo, S., D'Allessandro, W., 2014. High vanadium concentrations in groundwater at El Hierro (Canary Islands, Spain). 10th International Hydrogeological Congress of Greece, Thessaloniki, pp. 427–435.
Magaritz, M., Luzier, J.E., 1985. Water-rock interactions and seawater-freshwater mixing effects in the coastal dunes aquifer, Coos Bay, Oregon. Geochimica Cosmochimica Acta 49, 2515–2525.
Maloszewski, P., Zuber, A., 1985. On the theory of tracer experiments in fissured rocks with a porous matrix. J. Hydrol. 79, 333–358.
Maloszewski, P., Stichler, W., Zuber, A., 2004. Interpretation of environmental tracers in groundwater systems with stagnant water zones. Isot. Environ. Health Stud. 40, 21–33. http://dx.doi.org/10.1080/10256010310001645717.
Matthess, G., 1982. The Properties of Groundwater. John Wiley & Sons, New York.
MED-EUWI, 2007. Mediterranean groundwater report: Technical report on groundwater management in the mediterranean and the water Framework directive. Jt. Mediterr. EUWI/WFD Process, E. U. http://www.semide.net/initiatives/medeuwi/JP/GroundWater, 120 pages.
Meteorological Service, 2010. Meteorological Data Archive, Lebanon Weather, 1985-2010. Unpublished Weather Reports from Beirut International Airport Weather Station. General Directorate of Civil Aviation, Beirut, Lebanon.
Mondal, N.C., Singh, V.S., Puranik, S.C., Singh, V.P., 2010. Trace element concentration in groundwater of Pesarlanka island, Krishna delta, India. Environ. Monit. Assess. 163, 215–227. http://dx.doi.org/10.1007/s10661-009-0828-6.
Nader, F.H., 2000. Petrographic and Geochemical Characterization of the Jurassic-cretaceous Carbonate Sequence of the Nahr Ibrahim Region, Lebanon. M.S. Thesis. American University of Beirut, Lebanon.
Nader, F.H., Abdel-Rahman, A.M., Haidar, A.T., 2006. Petrographic and chemical traits of Cenomanian platform carbonates (central Lebanon): implications for depositional environments. Cretac. Res. 27, 689–706. http://dx.doi.org/10.1016/j.cretres.2006.03.009.
O'Connor, A.E., Luek, J.L., McIntosh, H., Beck, A.J., 2015. Geochemistry of redox-sensitive trace elements in a shallow subterranean estuary. Mar. Chem. 172, 70–81. http://dx.doi.org/10.1016/j.marchem.2015.03.001.
Parkhurst, D.L., Appelo, C.A.J., 1999. User's Guide to PHREEQC (Version 2), a Computer Program for Speciation, Batch-reaction, One-dimensional Transport, and Inverse Geochemical Calculations: U.S. Geological Survey Water-Resources Investigations Report 99–4259.
Parkhurst, D.L., Appelo, C.A.J., 2013. Description of Input and Examples for PHREEQC Version 3—a Computer Program for Speciation, Batch-reaction, One-dimensional Transport, and Inverse Geochemical Calculations. U.S. Geological Survey Techniques and methods, book 6, chap. A43. http://www.hydrochemistry.eu/ph3/manual3.pdf.
Perelman, A.I., 1972. Geochemie epigenetischer prozesse (die hypergene Zone). Akademie Verlag, Berlin.
Pichler, T., Mozaffari, A., 2015. Occurrence, distribution and mobility of geogenic molybdenum and arsenic in a limestone aquifer matrix. Appl. Geochem 63, 623–633. http://dx.doi.org/10.1016/j.apgeochem.2015.08.006.
Plummer, L.N., Back, W.W., 1980. The mass balance approach—application to interpreting the chemical evolution of hydrologic systems. Am. J. Sci. 280, 130–142.
Plummer, L.N., Prestemon, E.C., Parkhurst, D.L., 1994. An Interactive Code (NETPATH) for Modeling NET Geochemical Reactions along a Flow PATH, Version 2.0: U.S. Geological Survey Water-Resources Investigations Report 94–4169.
Porter, D.E., Michener, W.K., Siewicki, T., Edwards, D., Corbett, C., 1996. Geographic information processing assessment of the impacts of urbanization. In: Vernberg, F.J., Vernberg, W.B., Siewicki, T. (Eds.), Sustainable Development in the Southeastern Coastal Zone. Univ. South Carolina Press.
Post, V.E., 2002. 'Chemistry for Modellers' Aqueous Geochemistry in Coastal Areas. 17th Salt Water Intrusion Meeting. Deflt, The Netherlands, pp. 3–12.
Price, R.M., Herman, J.S., 1991. Geochemical investigation of salt-water intrusion into a coastal carbonate aquifer: Mallorca. Spain. Geol. Soc. Am. Bull. 103, 1270–1279.
Prommer, H., Barry, D.A., Zheng, C., 2003. MODFLOW/MT3DMS based reactive multi-component transport modelling. Ground Water 41 (2), 247–257.
Pulido-Leboeuf, P., 2004. Seawater intrusion and associated processes in a small coastal complex aquifer (Castell de Ferro, Spain). Appl. Geochem 19, 1517–1527. http://dx.doi.org/10.1016/j.apgeochem.2004.02.004.
Rezaei, M., Sanz, E., Raeisi, E., Ayora, C., Vázquez-Suñé, E., Carrera, J., 2005. Reactive transport modeling of calcite dissolution in the fresh-salt water mixing zone. J. Hydrol. 311, 282–298. http://dx.doi.org/10.1016/j.jhydrol.2004.12.017.
Saadeh, M., 2008. Influence of Overexploitation and Seawater Intrusion on the Quality of Groundwater in Greater Beirut. PhD Thesis. Aachen University, Germany.
Sacks, L.A., Tihansky, A.B., 1996. Geochemical and Isotopic Composition of Ground Water, with Emphasis on Sources of Sulfate, in the Upper Floridan Aquifer and Intermediate Aquifer System in Southwest Florida. U.S. Geological Survey, Water-Resources Investigations Report 96–4146.
Sanford, W.E., Konikow, L.F., 1989. Porosity development in coastal carbonate aquifers. Geol 17, 249–252.
Schulze-Makuch, D., 2005. Longitudinal dispersivity data and implications for scaling behavior. Ground Water 43 (3), 443–456. http://dx.doi.org/10.1111/j.1745-6584.2005.0051.x.
Shand, P., Edmunds, W.M., 2008. The baseline inorganic chemistry of European groundwaters. In: Edmunds, W.M., Shand, P. (Eds.), Natural Groundwater Quality. Blackwell Publishing Ltd, pp. 22–58.
Shi, J., Ma, R., Liu, J., Zhang, Y., 2013. Suitability assessment of deep groundwater for drinking, irrigation and industrial purposes in Jiaozuo City, Henan Province, north China. Chin. Sci. Bull. 58 (25), 3098–3110. http://dx.doi.org/10.1007/s11434-013-5952-6.
Simmons, C.T., Bauer-Gottwein, P., Graf, T., Kinzelbach, W., Kooi, H., Li, L., 2010. Variable density groundwater flow: from modelling to applications. In: Wheater, H.S., Mathias, S.A., Li, X. (Eds.), Groundwater Modelling in Arid and Semi-arid Areas, International Hydrology Series. Cambridge University Press, London, pp. 87–117.
Slama, F., 2010. Field Experimentation and Modelling of Salts Transfer in Korba Coastal Plain: Impact of Seawater Intrusion and Irrigation Practices. PhD Thesis.

University of Neuchatel, Centre of Hydrogeology.
Smedley, P.L., Edmunds, W.M., 2002. Redox patterns and trace-element behavior in the east midlands Triassic sandstone aquifer, UK. Ground Water 40, 44–58.
Smedley, P.L., Cooper, D.M., Ander, E.L., Milne, C.J., Lapworth, D.J., 2014. Occurrence of molybdenum in British surface water and groundwater: distributions, controls and implications for water supply. Appl. Geochem 40, 144–154. http://dx.doi.org/10.1016/j.apgeochem.2013.03.014.
Sola, F., Vallejos, A., Moreno, L., López, Geta, J.A., Pulido Bosch, A., 2013. Identification of hydrogeochemical process linked to marine intrusion induced by pumping of a semiconfined Mediterranean coastal aquifer. Int. J. Environ. Sci. Technol. 10, 63–76. http://dx.doi.org/10.1007/s13762-012-0087-x.
Stuyfzand, P.J., 1987. Influences of filtration and storage of groundwater samples on sample composition. Trends Anal. Chem. (TrAC) 6, 50–54.
Stuyfzand, P.J., 1993a. Hydrochemistry and Hydrology of the Coastal Dune Area of the Western Netherlands. Ph.D Thesis. Vrije Univ. Amsterdam, published by KIWA, The Netherlands.
Stuyfzand, P.J., 1993b. Behaviour of major and trace constituents in fresh and salt intrusion waters, in the Western Netherlands. In "Study and modelling of saltwater intrusion into aquifers. In: Custodio, E., Galofré, A. (Eds.), Proc. 12th Salt Water Intrusion Meeting, November 1992. CIHS. CIMNE Barcelona, Barcelona, pp. 143–160.
Stuyfzand, P.J., 1999. Patterns in groundwater chemistry resulting from groundwater flow. Hydrogeol. J. 7, 15–27.
Stuyfzand, P.J., 2011. Hydrogeochemical processes during riverbank filtration and artificial recharge of polluted surface waters: Zonation, identification, and quantification. In: Ray, Chittaranjan, Shamrukh, Mohamed (Eds.), Riverbank Filtration for Water Security in Desert Countries. Series: NATO Science for Peace and Security Series C: Environmental Security, first ed. Springer.
Stuyfzand, P.J., 2015a. Trace element patterns in Dutch coastal dunes after 50 years of artificial recharge with Rhine River water. Environ. Earth Sci. 73, 7833–7849. http://dx.doi.org/10.1007/s12665-014-3770-z.
Stuyfzand, P.J., 2015b. Hydrogeochemcal (HGC 2.2), for Storage, Management, Control, Correction and Interpretation of Water Quality Data in Excel® Spread Sheet. Nieuwegein: KWR report BTO 2012. 244(s).
Stuyfzand, PJ, Mendizabal, I., 2010. Trace element concentrations of groundwater from public supply well fields, and their relation with marine sedimentary environments of the aquifer and postdepositional salinity changes. Azores, Portugal SWIM 21st Salt Water Intrusion Meeting.
Sun, H., Alexander, J., Gove, B., Koch, 2015. Mobilization of arsenic, lead, and mercury under conditions of sea water intrusion and road deicing salt application. J. Contam. Hydrol. 180, 12–24. http://dx.doi.org/10.1016/j.jconhyd.2015.07.002.
Topal, T., Kaya, Y., 2016. Assessment of deterioration and collapse mechanisms of dolomitic limestone at Hasankeyf Antique City before and after reservoir impounding (Turkey). Environ. Earth Sci. 75 (131). http://dx.doi.org/10.1007/s12665-015-5062-7.
Tribovillard, N., Riboulleau, A., Lyons, T., Baudin, F., 2004. Enhanced trapping of molybdenum by sulfurized marine organic matter of marine origin in Mesozoic limestones and shales. Chem. Geol. 213 (4), 385–401.
Tulipano, L., Fidelibus, M.D., Panagopoulos, A., 2005. Groundwater Management of Coastal Karstic Aquifers; Final Report. COST Action 621, EUR 21366 (Luxembourg).
US EPA, 2008. EPA's Report on the Environment (ROE). U.S. Environmental Protection Agency, Washington, D.C. EPA/600/R-07/045F. Available online at: http://www.epa.gov/roe.
Van Genuchten, M. Th, 1985. A general approach for modeling solute transport in structured soils. Memoirs Int. Ass. Hydrogeol. 17 (2), 513–526.
Whitaker, F.F., Smart, P.L., 1993. Dolomitization by saline ground waters within the north-western great Bahama Bank: an overview. Proceedings of the sixth symposium on the geology of the Bahamas, pp. 165–179.
WHO, 2001. Beryllium and Beryllium Compounds. Concise International Chemical Assessment Document 32. WHO, Geneva.
WHO, 2008. Guidelines for Drinking-water Quality: Incorporating 1st and 2nd Addenda, vol. 1. Recommendations, 3rd edition. WHO, Geneva.
Wicks, C., Herman, J., 1995. The effect of zones of high porosity and permeability on the configuration of the saline-freshwater mixing zone. Groundwater 33 (5), 733–740.
Yan, Z., Chen, C., Fan, P., Wang, M., Fang, X., 2015. Pore structure characterization of ten typical rocks in China. Electron. J. Geotech. Eng. 20, 479–494.
Zghibi, A., Merzougui, A., Zouhri, L., Tarhouni, J., 2014. Understanding groundwater chemistry using multivariate statistics techniques to the study of contamination in the Korba unconfined aquifer system of Cap-Bon (North-east of Tunisia). J. Afr. Earth Sci. 89, 1–15. http://dx.doi.org/10.1016/j.jafrearsci.2013.09.004.